RSC Advances

PAPER

View Article Online
View Journal | View Issue

Cite this: *RSC Adv.*, 2025, **15**, 38670

Novel 2-substituted benzothiazole derivatives: synthesis, *in vitro* and *in silico* evaluations as potential anticancer agents

Rasha A. Azzam, [a] Mona M. Seif,[a] Maha A. El-Demellawy [bc] and Galal H. Elgemeie *[a]

Cancer remains a global health concern, demanding the development of new therapeutic medicines. This research focuses on the synthesis, *in vitro* evaluation, and *in silico* analysis of new 2-substituted benzothiazole derivatives as possible anticancer drugs. Hybrid molecules comprising benzothiazole and pyridinone rings **8a–c** and **10a–c** were also synthesized. Several compounds were produced and characterized, using NMR, IR and elemental analysis, with promising anticancer activity against lung H1299, liver Hepg2 and breast MCF7 cancer cell lines. Structure–activity connection investigations identified crucial structural characteristics that influence potency, with benzylidine derivatives **6a–g** demonstrating higher activity. *In silico* ADME research revealed favorable drug-like features for chosen compounds, such as high gastrointestinal absorption and selective CYP inhibition. Toxicological projections indicated few side effects, confirming their potential as medication candidates. Inverse-docking analysis of the five potent compounds **6a–c**, **6e**, and **6f** against 12 selected protein tyrosine kinases (PTKs) and cyclin-dependent kinases (CDKs) revealed good docking scores, strong interaction patterns, and potential inhibitory effects, particularly against ABL1, ABL2, CDK4, and CDK6 enzymes, suggesting these compounds as promising candidates for further drug development.

Received 9th May 2025
Accepted 2nd October 2025

DOI: 10.1039/d5ra03277f

rsc.li/rsc-advances

1. Introduction

Cancer is one of the deadliest diseases in the world, killing nearly 10 million people in 2020. When it comes to global mortality statistics, cancer is the second most common cause of death. The most prevalent causes of cancer mortality in 2020 are lung, colon, rectum, liver, stomach, and breast.[1,2] Over the last decade, cancer-related deaths have increased by 28%, much outpacing the 9% increase in general mortality rates.[3] Cancer death rates vary among regions due to a mix of hereditary and environmental factors. These factors influence the effectiveness of screening campaigns, preventive measures, and treatment options for distinct forms of cancer.[4] The ongoing evolution of medical technologies holds up the possibility of improved screening capabilities as well as, more importantly, advancements in patient care and treatment options. For example, much emphasis has been put on anti-cancer research for developing effective agents, especially compounds that contain benzothiazole and 2-pyridinone moiety.[5–8] Several studies have been undertaken to improve the anti-cancer activity of benzothiazole by synthesizing a wide range of derivatives. Among these compounds, 2-arylbenzothiazole derivatives have shown promising antitumor activity. For instance, CJM 126, 2-(4-aminophenyl)-benzothiazole **A**, had excellent *in vitro* cytotoxicity in nanomolar concentrations and caused potent growth inhibition against human-derived breast carcinoma cell lines, including estrogen receptor-positive (ER+) MCF-7wt cells.[9] Additionally, PMX-610, 2-(3,4-dimethoxyphenyl)-5-fluorobenzothiazole **B**, demonstrated superior *in vivo* efficacy against human breast cancer cell lines MCF-7 and MDA-468 in nanomolar concentrations; however, high lipophilicity restricted its *in vivo* development in aqueous formulations and apparently prevented its development as a chemotherapeutic agent.[10] SAR study of compound **B** revealed that the presence of a methoxy substituent at carbon 3 and 4 of the phenyl ring was important for its antitumor activity; replacing this group with another one resulted in the loss of activity. To overcome this problem, fluorinated analog, 4-(5-fluorobenzothiazol-2-yl)-2-methylaniline **C**, DF 203, has been developed and resolved the metabolic issues.[11] Compound **C** showed potent antitumor activity against wide spectrum of cancers such as ovarian, breast, collateral, and kidney, Fig. 1.[12]

[a]*Chemistry Department, Faculty of Science, Helwan University, Cairo, Egypt. E-mail: elgemeie@yahoo.com*

[b]*Pharmaceutical and Fermentation Industries Development Centre (PFIDC), The City of Scientific Research and Technological Applications (SRTA-City), Borg Al-Arab, Alexandria, Egypt*

[c]*Medical Biotechnology Department, Genetic Engineering & Biotechnology Research Institute (GEBRI), City of Scientific Research & Technological Applications (SRTA-City), New Borg El-Arab City, Alexandria, Egypt*

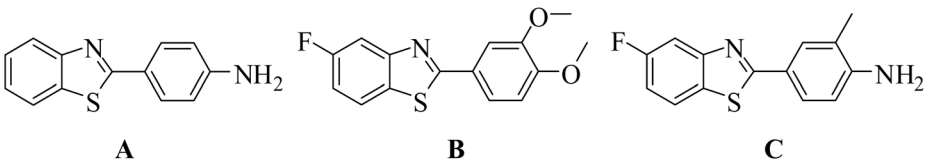

Fig. 1 Examples of potent anticancer benzothiazole derivatives.

Previous research has demonstrated that benzothiazole containing compounds exhibit significant antiproliferative and apoptotic effects on various cancer types, including those of the lung, liver, and breast origin. For instance, studies have shown that substituted benzothiazoles can inhibit the growth of HepG2 liver cancer cells and MCF7 breast cancer cells by inducing apoptosis and disrupting the cell cycle.[13,14] Similarly, the anticancer activity of benzothiazole derivatives has been documented in lung cancer cell lines, such as H1299, by inhibiting cell proliferation and migration.[15]

Protein tyrosine kinases (PTKs) are crucial enzymes involved in cellular signaling, and their dysregulation is a significant factor in cancer development and progression.[16] Benzothiazole derivatives have been identified in literature as a class of compounds that can act as potent inhibitors of PTKs.[17] The benzothiazole scaffold is known to mimic the adenine portion of ATP, allowing it to compete for binding at the catalytic domain of these kinases.[18] This competitive inhibition prevents the kinases from performing their normal function of phosphorylating proteins, thus disrupting critical pro-cancer signaling pathways. Specifically, several studies have shown that substituted benzothiazoles can inhibit a variety of PTKs, including ABL1 and ABL2 kinases.[19] By blocking the activity of these molecular targets, benzothiazole compounds can effectively inhibit the proliferation and survival of cancer cells.

Over the last two decades, there has been a surge of interest in 2-pyridone derivatives in medicinal development efforts, with numerous FDA-approved medications working as kinase inhibitors. These include recent approvals for Tazemetostat (2020), which stands up as an effective, selective, and orally accessible small-molecule inhibitor of EZH2.[20] This is crucial because EZH2 inhibitors have promises in cancer treatment, especially in tackling difficulties such as drug resistance, poor distribution, and limited brain penetration reported with several current chemotherapeutic medications, Fig. 2. Additionally, Fredericamycin A is being investigated as a new lead molecule for battling human tumours,[21] whilst Camptothecin has been proven to be effective in cancer treatment by blocking DNA topoisomerase I,[22] Fig. 2.

Several 2-(benzo[*d*]thiazol-2-yl)acetohydrazide derivatives have been developed[23,24] and used for the synthesis of benzothiazole hybrid compounds.[25–27] Drawing on our previous successes in developing compounds containing benzothiazole and pyridinone rings, which demonstrated significant antimicrobial[28–30] and antiviral activities,[31–34] we proceeded on a new venture. Building on this foundation, we synthesized new benzothiazole hydrazide and benzylidine derivatives as well as hybrid compounds containing both benzothiazole and pyridinone and tested their potential anticancer properties. Furthermore, we conducted extensive *in-silico* research and docking analysis to better understand the molecular mechanisms behind their interactions and

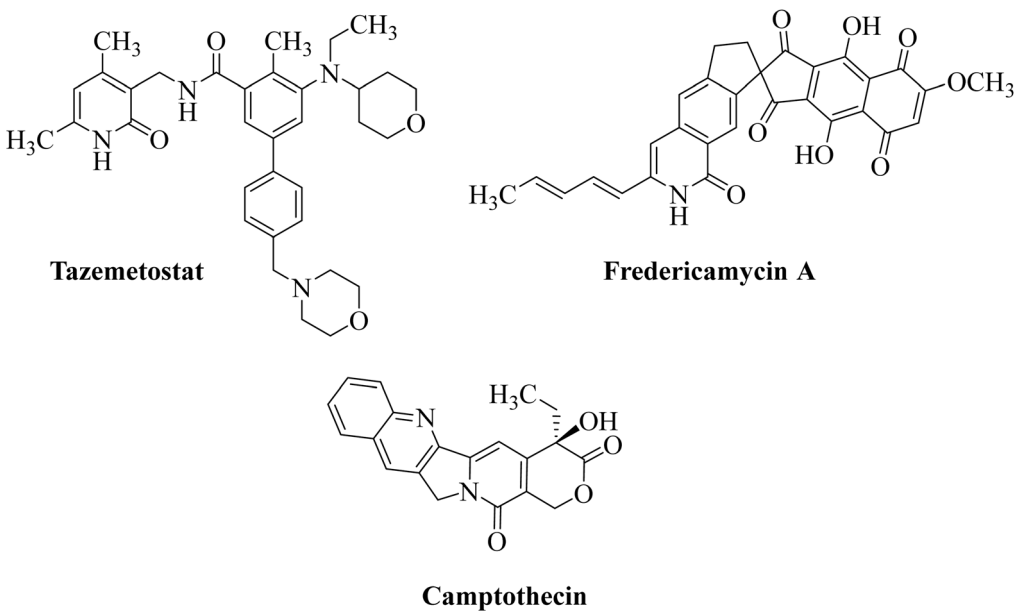

Fig. 2 Anticancer drugs containing 2-pyrdinone.

efficacy. After that, an inverse docking process was applied to the most active compounds to choose prospective molecular targets from a list of ones that are frequently dysregulated in cancer. This holistic strategy seeks to advance our understanding of these chemicals' therapeutic potential in cancer treatment, establishing the framework for future drug development initiatives.

2. Results and discussions

2.1. Chemistry

Novel *N*′-(2-(benzo[*d*]thiazol-2-yl)acetyl)benzohydrazide derivatives **4a–e** were first synthesized and subsequently employed in the preparation of new benzothiazole derivatives *N*′-(2-(benzo[*d*]

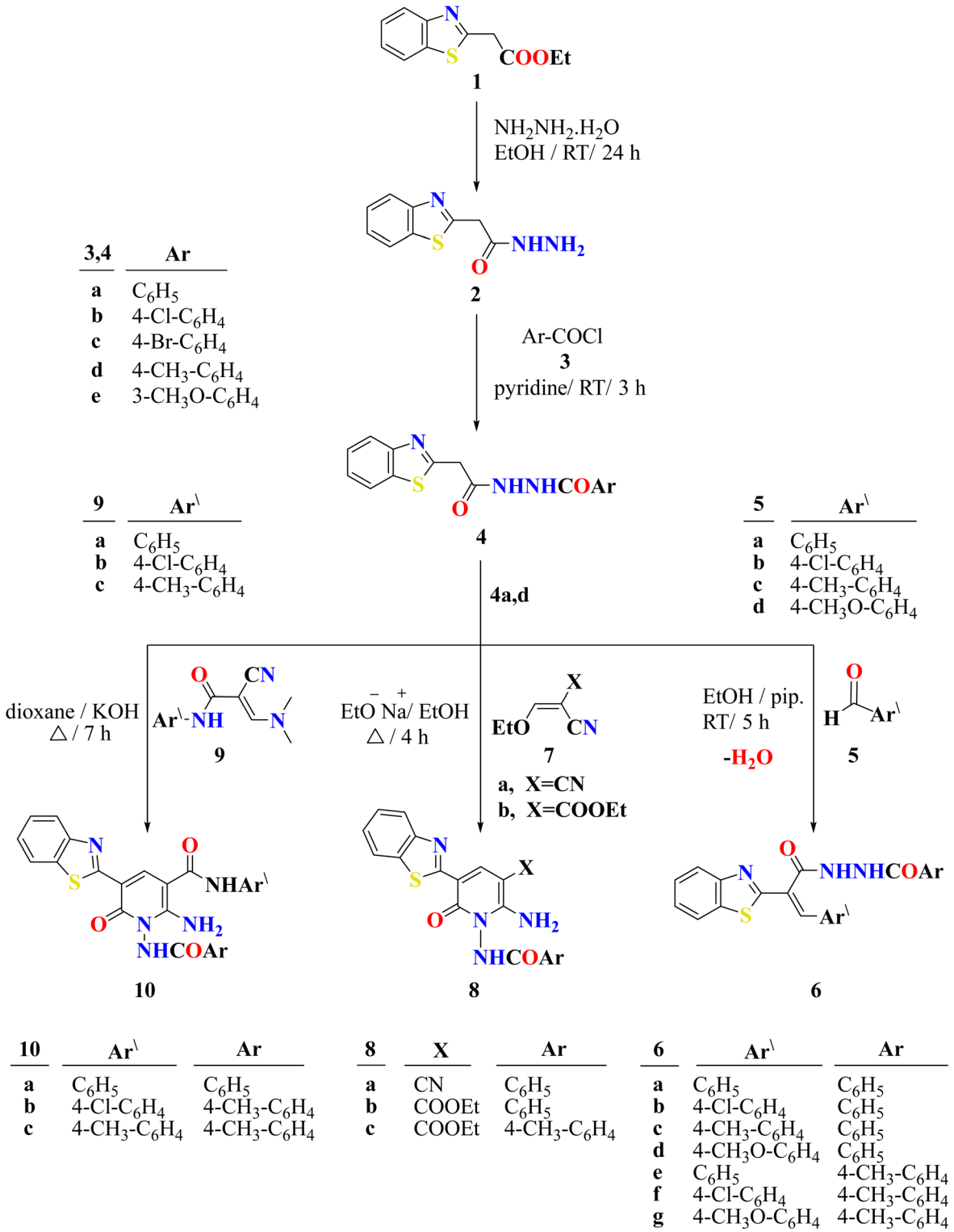

3,4	Ar
a	C_6H_5
b	4-Cl-C_6H_4
c	4-Br-C_6H_4
d	4-CH_3-C_6H_4
e	3-CH_3O-C_6H_4

9	Ar\
a	C_6H_5
b	4-Cl-C_6H_4
c	4-CH_3-C_6H_4

5	Ar\
a	C_6H_5
b	4-Cl-C_6H_4
c	4-CH_3-C_6H_4
d	4-CH_3O-C_6H_4

10	Ar\	Ar
a	C_6H_5	C_6H_5
b	4-Cl-C_6H_4	4-CH_3-C_6H_4
c	4-CH_3-C_6H_4	4-CH_3-C_6H_4

8	X	Ar
a	CN	C_6H_5
b	COOEt	C_6H_5
c	COOEt	4-CH_3-C_6H_4

6	Ar\	Ar
a	C_6H_5	C_6H_5
b	4-Cl-C_6H_4	C_6H_5
c	4-CH_3-C_6H_4	C_6H_5
d	4-CH_3O-C_6H_4	C_6H_5
e	C_6H_5	4-CH_3-C_6H_4
f	4-Cl-C_6H_4	4-CH_3-C_6H_4
g	4-CH_3O-C_6H_4	4-CH_3-C_6H_4

Scheme 1 Synthesis of 2-substituted benzothiazole derivatives.

thiazol-2-yl)-3-arylacryloyl)benzohydrazide derivatives **6a–g**, *N*-(6-amino-3-(benzo[*d*]thiazol-2-yl)-2-oxopyridin-1(2*H*)-yl)benzamide derivatives **8a–c** and 2-amino-1-benzamido-5-(benzo[*d*]thiazol-2-yl)-6-oxo-*N*-aryl-1,6-dihydropyridine-3-carboxamide derivatives **10a–d**, as illustrated in Scheme 1.

The starting compound 2-(benzo[*d*]thiazol-2-yl) acetohydrazide **2** was obtained by reacting to hydrazine hydrate with ethyl 2-(benzo[*d*]thiazol-2-yl)acetate **1** in ethanol at room temperature for 24 hours.[32] As illustrated in Scheme 1, benzothiazole hydrazide **2** was then reacted with benzoyl chloride derivatives **3a–e** in the presence of pyridine at room temperature to afford the target *N*′-(2-(benzo[*d*]thiazol-2-yl) acetyl)benzohydrazide **4a–e**. The reaction proceeded *via* nucleophilic substitution of the chloride atoms in benzoyl chloride by the hydrazide NH_2 group. The structures of the synthesized compounds were confirmed by elemental analysis and spectrum data such as IR, ^{1}H NMR, and ^{13}C NMR. The IR spectra of compounds **4a–e** revealed a broad absorption band at 3439–3175 cm^{-1} corresponding to the NH group and two characteristic bands at 1696–1602 cm^{-1} attributable to two C=O groups. Moreover, the ^{1}H NMR spectrum of compound **4a** showed a singlet signal at δ 4.23 ppm, confirming the presence of a CH_2 group as well as four characteristic signals corresponding to the four protons of benzothiazole ring; two triplets at δ 7.43 and 7.58 ppm and two doublets at δ 7.98 and 8.06 ppm. In addition, the ^{1}H NMR showed multiplet signal at a range of δ 7.49–7.53 ppm and one doublet signal at δ 7.91 ppm corresponding to the five protons of benzene ring. The ^{13}C NMR spectrum of compound **4a** further supported the proposed structure, showing a CH_2 group at δ 39.4 ppm and two carbon atoms of C=O groups at δ 165.9 and 167.1 ppm. To confirm the structure of *N*′-(2-(benzo[*d*]thiazol-2-yl)acetyl)benzohydrazide derivatives **4** unambiguously, the X-ray crystal structure of **4a** was determined, Fig. 3.[24]

Following the preparation of *N*′-(2-(benzo[*d*]thiazol-2-yl) acetyl)benzohydrazide derivatives **4a–e**, the corresponding benzilydine derivatives were prepared *via* Knoevenagel condensation of benzaldehyde derivatives **5a–d** with compounds **4a,d**. In this process, piperidine deprotonated the active methylene group in compound **4**, enabling nucleophilic attack on the carbonyl group of benzaldehyde **5**, followed by dehydration to afford *N*′-(2-(benzo[*d*]thiazol-2-yl)-3-arylacryloyl) benzohydrazide derivatives **6a–g** in good yields (Scheme 1). The structures of compounds **6a–g** were confirmed by their spectroscopic analysis such as IR, ^{1}H NMR and ^{13}C NMR. The IR spectrum of compound **6b** exhibited a broad absorption band at 3438 cm^{-1} due to the NH group, along with sharp absorption bands at 1692 and 1644 cm^{-1} corresponding to the two C=O groups. The ^{1}H NMR spectrum of **6b** displayed a singlet at δ 7.75 ppm for the CH proton and two singlets at δ 10.74 and 10.78 ppm for the two NH groups. Additionally, the ^{13}C NMR spectrum of **6b** revealed two characteristic resonances at δ 166.2 and 166.4 ppm, attributable to the two C=O carbons.

To confirm the structure of the resulting benzylidene product, 2D NMR techniques for compound **6d**, including ^{1}H–^{1}H COSY, ^{1}H–^{13}C HSQC, and ^{1}H–^{13}C HMBC, were performed, Fig. 4A–C. The ^{1}H–^{1}H COSY spectrum revealed a strong correlation between the benzothiazole proton at 7.46 ppm and proton at 8.12 ppm, as well as the proton at 7.46 ppm and proton at 8.00 ppm, indicating spin coupling within the system. Additionally, a significant correlation was observed between the benzene ring protons adjacent to the methoxy (–OMe) group at 7.95 ppm and those at 7.00 ppm, further supporting the structural connectivity.

N′-(2-(benzo[*d*]thiazol-2-yl)acetyl)benzohydrazide derivatives **4a,d** were reacted with ethoxymethylene compounds, 2-(ethoxymethylene)malononitrile **7a** and (*E*)-ethyl 2-cyano-3-ethoxy-acrylate **7b** to afford *N*-(6-amino-3-(benzo[*d*]thiazol-2-yl)-5-cyano-2-oxopyridin-1(2*H*)-yl)benzamide **8a** and ethyl 2-amino-1-benzamido-5-(benzo[*d*]thiazol-2-yl)-6-oxo-1,6-dihydropyridine-3-carb-oxylate **8b,c**, respectively, Scheme 1. The reaction was carried out in ethanol using one equivalent of potassium hydroxide. The mechanism likely involves a Michael addition of the ethoxymethylene compounds to **4a,d**, followed by ethanol elimination and intramolecular cyclization through nucleophilic attack of the NH group on the cyano group, ultimately yielding the *N*-arylcarbamide pyridone derivatives **8a–c**. The elemental analysis and spectral data confirmed the proposed structure of compounds **8a–c**. For example, IR spectrum of compound **8a** displayed absorption band at ν 3430 cm^{-1} for NH_2 group, as well as a band at ν 2216 cm^{-1} corresponding to the CN group and band at ν 1631 cm^{-1} corresponding to C=O group. The ^{1}H NMR spectra of **8a–c** displayed singlets at δ 8.72–8.76 ppm and δ 9.10–9.21 ppm corresponding to the pyridone CH protons of **8a** and **8b,c**, respectively. In addition, the spectra of **8b,c** exhibited characteristic signals for the ethyl group: a triplet at δ 1.13–1.16 ppm (CH_3) and a quartet at δ 3.96–4.38 ppm (CH_2). The ^{13}C NMR spectrum of **8a** showed resonances at δ 118.6, 162.1, and 164.1 ppm, consistent with CN and two C=O carbons, respectively.

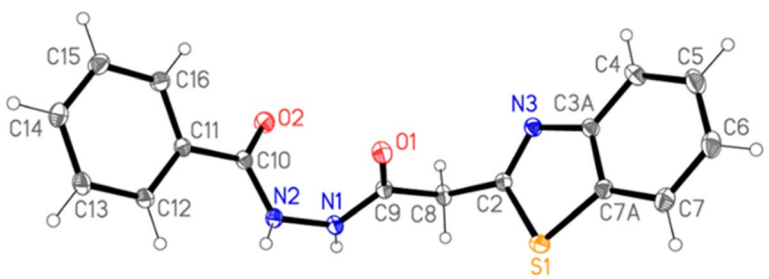

Fig. 3 The structure of compound **4a** in the crystal.[24]

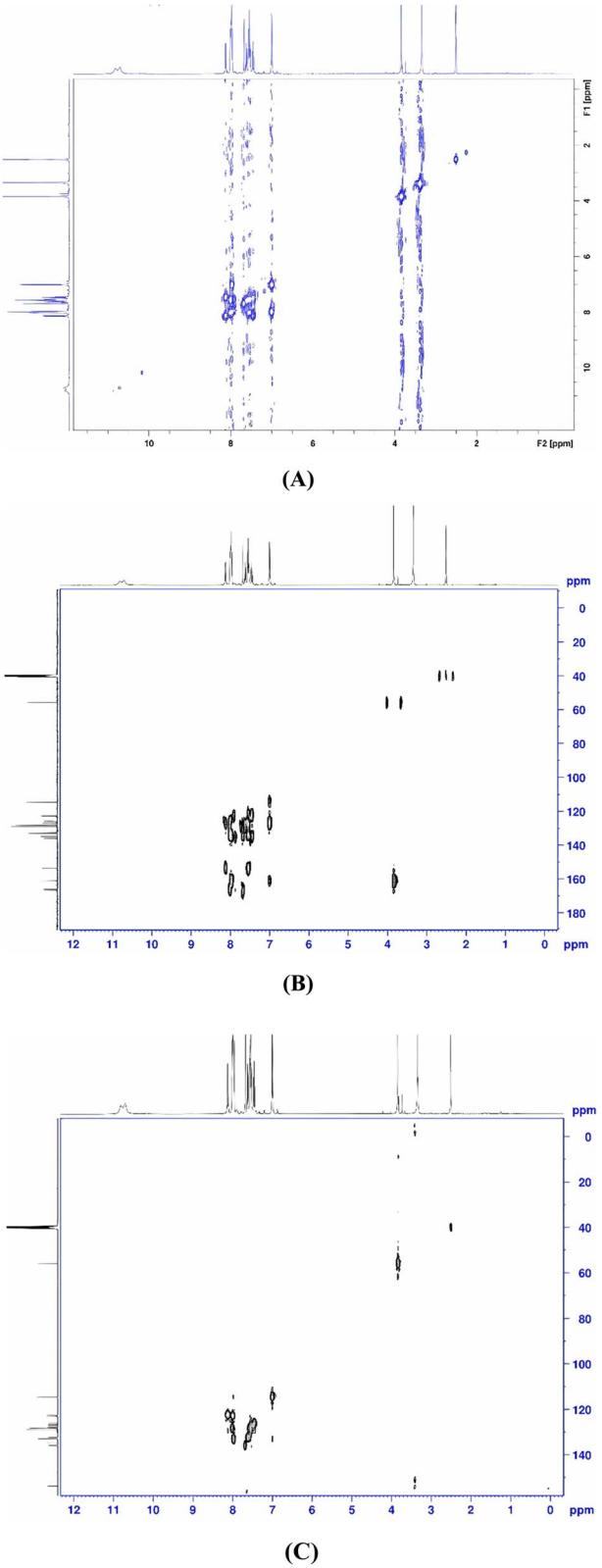

Fig. 4 2D NMR of compound **6d**, (A) COSY; (B) HMBC; (C) HSQC.

The target derivatives of 2-amino-1-benzamido-5-(benzo[*d*]thiazol-2-yl)-6-oxo-*N*-phenyl-1,6-dihydropyridine-3-carboxamide derivatives **14a–c** were synthesized by reacting **4a,d** with *N*-phenyl acrylamide derivatives **9a–c** in basic condition, Scheme 1. The reaction proceeded *via* a Michael addition, followed by elimination of $NH(CH_3)_2$ and subsequent intramolecular cyclization through nucleophilic attack of the NH proton on the cyano group, affording the desired products **10a–c**. The structures of compounds **10a–c** were confirmed by IR, ^{1}H NMR and ^{13}C NMR and elemental analysis. According to the IR spectral analysis of compounds **10a–c**, the appearance of an absorption band at a range of 3489–3327 cm^{-1} confirmed the presence of NH group. In addition, the IR spectra showed a sharp band at a range of 1660–1623 cm^{-1} which corresponds to C=O group. The ^{1}H NMR of compound **10b**, as an example, showed three singlet signals which assigned for the protons of CH_3 group, CH group of pyridone and NH group at δ 2.42, 9.23 and 11.68 ppm, respectively. ^{1}H NMR of compound **10c** displayed four characteristic signals corresponding to the four protons of benzothiazole ring, two triplet signals at δ 7.26 and 7.44 ppm and two doublets at δ 7.92 and 8.02 ppm in addition to four doublet signals for two aryl groups. Additionally, the ^{13}C NMR spectrum of **10b** confirmed the presence of CH_3 carbon δ 21.5 ppm and two C=O carbons at δ 162.5 and 165.0 ppm.

2.2. Biological activity

2.2.1 Anticancer activity. Compounds **4a–e**, **6a–g**, **8a–c**, **10b**, and **10c** were evaluated *in vitro* for their anticancer activity against three human cancer cell lines—lung (H1299), liver (HepG2), and breast (MCF7)—using the SRB assay, with doxorubicin as the standard drug. Cytotoxicity was evaluated at four

Table 1 Cytotoxic activity (IC_{50}, μM) of synthesized benzothiazole derivatives against three human cancer cell lines compared with doxorubicin

Compound	H1299	HEPG2	MCF7
Doxorubicin[a]	**7.87**	**8.70**	**7.69**
4a	>50[b]	>50[b]	>50[b]
4b	>50	>50	>50
4c	>50	>50	>50
4d	>50	>50	>50
4e	>50	>50	>50
6a	>50	**12.52**	15.02
6b	>50	25.35	**12.67**
6c	>50	**12.57**	**14.51**
6d	>50	>50	>50
6e	>50	**10.88**[c]	**24.18**
6f	>50	**10.00**[c]	**16.74**
6g	>50	36.07	33.82
8a	>50	>50	>50
8b	>50	>50	27.62
8c	>50	>50	>50
10b	>50	>50	>50
10c	>50	>50	>50

[a] Doxorubicin was included as the positive control and standard reference drug. [b] Values reported as ">50 μM" indicate no measurable activity at the highest tested concentration. [c] Bold values denote compounds with $IC_{50} \leq 15$ μM, considered comparable to the reference drug in potency.

different concentrations, and the IC_{50} values of the tested compounds were compared to those of the reference drug, as presented in Table 1. Additionally, the surviving fraction was measured and compared with the control group. Anti-cancer activities of the synthesized compounds have shown low activity against lung H1299 cell line. While no compound exhibited higher activities than standard drugs, doxorubicin (DOX), with H1299, benzylidine derivatives **6a–c**, **6e** and **6f** showed comparable results with standard drug against Hepg2 and MCF7 cell lines. Additionally, only benzylidine compounds **6a–g** have shown high activities than starting benzoyl derivatives **4a–e** as well as other compounds that have benzothiazole bonded with pyrdinone ring **8a–c**, **10b** and **10c** against the three tested cell lines.

Based on IC_{50} values of the synthesized compounds against lung H1299, liver Hepg2 and breast MCF7 cancer cell lines, as shown in Table 1, the structure–activity relationships (SAR) were established. For instance, both compounds **6a** and **6c** with benzoyl group and either hydrogen atom or methyl group at C4 at the benzene ring, respectively, have shown almost equal activities toward liver Hepg2 (IC_{50} = 12.52 and 12.56 μM) and breast MCF7 cell lines (IC_{50} = 15.02 and 14.51 μM). However, introducing chlorine atom to benzene ring, compound **6b**, led to decreasing the activity against the liver Hepg2 cell line and increasing activity against the breast MCF7 cell line (IC_{50} = 25.35 and 12.67 μM, respectively). On the other hand, the presence of methoxy group at the para position of benzene ring, compound **6d**, led to decreasing the activity against liver Hepg2 and breast MCF7 cell lines (IC_{50} = 50+ μM). Alternatively, the presence of 4-methylbenzoyl group and either hydrogen or chlorine atom at C4 of the benzene ring, compounds **6e** and **6f**, resulted in lower activities for these compounds against the breast MCF7 cell line (IC_{50} = 24.18 and 16.74 μM, respectively) as compared to the corresponding compounds containing non-substituted benzoyl group, **6a** and **6b**. Surprisingly compounds **6e** and **6f**, gave the highest activities against the liver Hepg2 cell line (IC_{50} = 10.88 and 10.00 μM, respectively). Introducing the methoxy group at the para position of benzene ring, compound **6g**, resulted in decreasing the activity against liver Hepg2 and breast MCF7 cell lines (IC_{50} = 36.07 and 33.82 μM, respectively). The mentioned data indicated that compounds **6e** and **6f** are the most potent against liver Hepg2 as compared to doxorubicin drug (IC_{50} = 8.70 μM).

2.2.2 Pass prediction. The PASS computer program offers a means to predict the potential biological activity profile of drug-like organic compounds based on their structural formula. This estimation relies on an analysis of structure–activity relationships derived from a comprehensive training set encompassing pharmaceutical agents, chemical probes, compounds with known toxicity data, drug substances, and candidates at various stages of clinical and preclinical investigation. Biological activity is categorized as either "active" or "inactive" (Pa and Pi are ranging from zero to one for each activity category) within the PASS program. Notably, compounds **6a–g** exhibited the highest anticancer activity among the synthesized compounds (as depicted in Table 2), surpassing other activities such as antitubercular, antimycobacterial, and anticonvulsant effects.

2.2.3 *In silico* ADME study

2.2.3.1 Physicochemical, pharmacokinetic/ADME and drug likeness properties. The synthesized compounds' potential as drug candidates was explored through an *in silico* ADME study using the Swiss ADME online tool. Physicochemical and pharmacokinetic properties of the most potent five compounds, **6a–c**, **6e**, and **6f**, were evaluated (Table S1, SI Document). A molecule's poor oral bioavailability in drug discovery is often associated with more than five hydrogen bond donors, ten hydrogen bond acceptors, a molecular weight exceeding 500 g mol^{-1}, and a calculated LogP above 5. Notably, the molecular weights of all

Table 2 The predicted biological activities spectrum of synthesized compounds by pass analysis Pa, Pi

	Antituberculosic		Antimycobacterial		Anticonvulsant		Antineoplastic	
Comp. No.	Pa	Pi	Pa	Pi	Pa	Pi	Pa	Pi
4a	0.302	0.069	0.344	0.057	0.315	0.112	0.322	0.140
4b	0.279	0.083	0.335	0.061	0.387	0.070	0.222	0.209
4c	0.365	0.043	0.436	0.031	0.350	0.088	0.325	0.138
4d	0.305	0.067	0.348	0.056	0.287	0.129	0.307	0.148
4e	0.286	0.078	0.353	0.054	NA	NA	0.362	0.120
6a	0.360	0.045	0.410	0.037	0.213	0.182	0.714	0.024
6b	0.336	0.055	0.399	0.039	0.296	0.123	0.584	0.049
6c	0.363	0.044	0.414	0.036	NA	NA	0.673	0.031
6d	0.337	0.054	0.415	0.035	NA	NA	0.682	0.029
6e	0.363	0.044	0.414	0.036	NA	NA	0.673	0.031
6f	0.340	0.053	0.403	0.038	0.270	0.141	0.547	0.058
6g	0.341	0.052	0.419	0.035	NA	NA	0.648	0.035
8a	0.388	0.035	0.256	0.114	0.477	0.041	NA	NA
8b	0.506	0.012	0.425	0.033	0.621	0.016	NA	NA
8c	0.506	0.012	0.426	0.033	0.588	0.021	NA	NA
10a	0.476	0.015	0.393	0.041	0.582	0.022	0.276	0.167
10b	0.456	0.018	0.386	0.043	0.631	0.015	NA	NA
10c	0.480	0.014	0.397	0.040	0.554	0.026	0.269	0.172

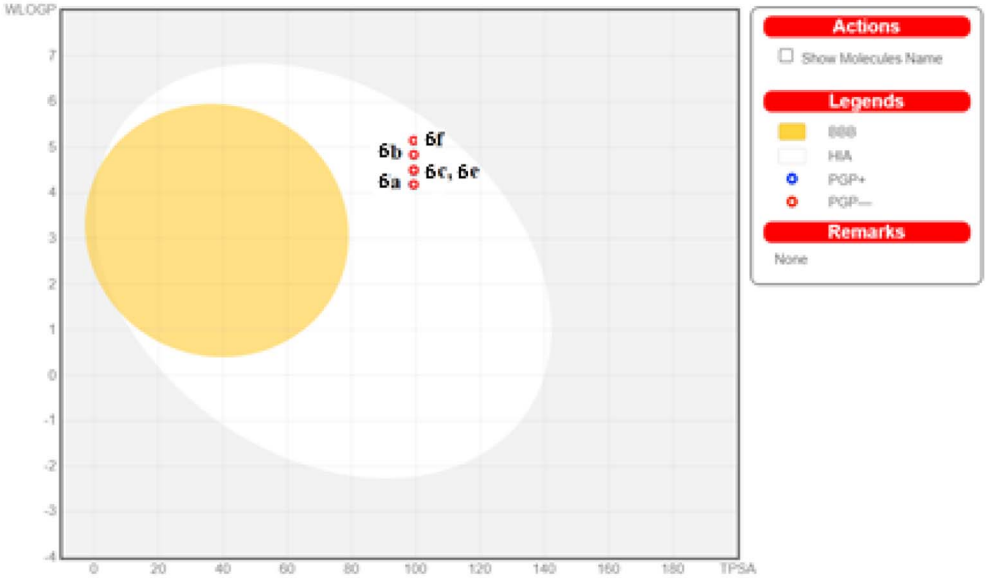

Fig. 5 BOILED-EGG diagram of tested compounds **6a–c**, **6e** and **6f**.

tested compounds range from 399.46 g mol^{-1} to 447.94 g mol^{-1} which indicates good bioavailability. These compounds showed moderate numbers of hydrogen bond acceptors and donors, three and two respectively, suggesting potential hydrogen bonding interactions with biological targets. The iLogP values, ranging from 3.1 to 3.6, indicated moderate lipophilicity, essential for drug-like properties. Three compounds, **6a**, **6c** and **6e** showed moderate solubility while two compounds that have chlorine atom, **6b** and **6e**, showed poor solubility. Topological polar surface area (TPSA) of all tested compounds exhibited the same value of 99.33 $Å^2$, which is lower than 140 and indicated good oral bioavailability. Additionally, the predicted high gastrointestinal absorption (GI absorption) of the compounds suggests good potential for oral administration. BOILED-EGG diagram displayed the bioavailability property space for wlogP and TPSA, white area means that intestinal absorption, Fig. 5. All compounds are failed in the white area which suggests these molecules have lower affinity or interaction with P-gp. In the context of bioavailability, P-gp-compounds may have higher absorption rates or lower susceptibility to efflux by P-gp, leading to potentially higher bioavailability. Lack of blood–brain barrier (BBB) penetration of all five potent compounds indicates no central nervous system effects, while non-substrate predictions for P-glycoprotein suggest positive drug absorption and distribution. Moreover, potent benzothiazole derivatives inhibited CYP2C19 and CYP2C9 but not CYP1A2, CYP2D6, or CYP3A4, implying selective CYP inhibition with potential drug–drug interaction relevance. Poor skin permeability is predicted for these compounds due to the negative log K_p values. With adherence to Lipinski, Ghose, Vebe, and Egan's rules for drug-likeness, except for one Muegge violation indicating good oral bioavailability, the compounds exhibited a consistent bioavailability score of 0.55, suggesting moderate potential for oral bioavailability.

2.2.4 Toxicological properties. The *in silico* predictions of toxicological properties of **6a–c**, **6e** and **6f** compounds were determined using the Osiris property explorer program available online at **http://www.propertyexplorer-cheminfo.org** and summarized in Table 3. The results showed that all five compounds are predicted to be non-mutagenic and non-tumorigenic. This suggests they are unlikely to cause genetic mutations or cancer. Similarly, none of the compounds are expected to be irritants, indicating they may not cause skin or eye irritation. The compounds are also predicted to have no reproductive effects, meaning they are unlikely to interfere with reproductive health or fetal development. Druglikeness assesses how well a compound resembles known drugs in terms of its physicochemical properties. Scores above zero generally indicate drug-like characteristics. Here, all compounds show positive druglikeness scores, ranging from 2.73 to 5.88. This suggests they possess properties that could make them suitable as drugs. Drug score evaluates the overall potential of a compound to be developed as a drug, considering various factors like druglikeness and toxicity risks. The drug scores for these compounds range from 0.69 to 0.81. While these values are not exceptionally high, they still indicate some potential for drug development, especially when combined with the absence of predicted mutagenicity, tumorigenicity, and irritant effects.

Table 3 Toxicity prediction of compounds **6a–c**, **6e** and **6f**

Compounds	6a	6b	6c	6e	6f
Mutagenic	No	No	No	No	No
Tumorigenic	No	No	No	No	No
Irritant	No	No	No	No	No
Reproductive effective	No	No	No	No	No
Druglikeness	4.09	5.88	3.75	2.73	4.39
Drug score	0.81	0.74	0.77	0.76	0.69

Table 4 Inverse docking studies of the potent compounds **6a–c**, **6e**, and **6f**

Target enzyme (PDB)		6a	6b	6c	6e	6f	DOX	Co-crystalline ligand
Non-receptor tyrosine kinases								
								1N1
ABL1 (2GQG)	Docking score (kcal mol^{-1})	−8.7770	−8.8507	−8.8166	−8.6343	−8.7165	−6.0284	−9.2914
	Types of interactions	H-bond	H-bond	H-bond	H-bond Arene	H-bond Arene	2 H-bond	3 H-bond Arene
	Residues	Met318	Met318	Met318	Met318 Asp381	Met318 Asp381	Thr319, Tyr320	2 Met318, Thr315 Leu248
								DKI
ABL2 (3HMI)	Docking score (kcal mol^{-1})	−6.0677	−6.0620	−6.0978	−6.1215	−6.1636	−4.8389	−7.5292
	Types of interactions	2 H-bond Arene	2 H-bond Arene	2 H-bond Arene	H-bond Arene	H-bond Arene	—	3 H-bond Arene
	Residues	Met354, Asp371 Gly296	Met354, Asp371 Gly296	Met354, Asp371 Gly296	Asp371 Gly296	Asp371 Gly296	—	Glu362, Gly296, Met364 Thy299
								H82
PTK2 (6I8Z)	Docking score (kcal mol^{-1})	−7.9650	−6.3871	−7.1521	−7.0425	−7.1957	−5.7019	−11.1462
	Types of interactions	Arene	2 H-bond	3 H-bond Arene	Arene	3 H-bond Arene	3 H-bond	5 H-bond
	Residues	Arg426	2 Glu506	2 Glu506, Arg246 Asn551	Arg426	2 Glu506, Arg246 Asn551	Glu506, Gly505, Arg426	2 Cys502, Lie428, Glu500, Asp564
								T74
CDC42 (3EQR)	Docking score (kcal mol^{-1})	−8.1533	−8.1731	−8.2297	−7.9906	−8.3175	−5.2157	−11.5928
	Types of interactions	Arene	Arene	Arene	—	Arene	Arene	4 H-bond
	Residues	Thr205	Thr205	Thr205	—	Thr205	Leu122	2 Ala208, Glu205, Thr205
								FLJ
PTK6 (6CZ3)	Docking score (kcal mol^{-1})	−6.5834	−6.6710	−6.2771	−6.6924	−6.7636	−5.5634	−9.12444
	Types of interactions	H-bond Arene	H-bond Arene	Arene	H-bond Arene	H-bond Arene	2 H-bond Arene	4 H-bond Arene
	Residues	Met267 Leu197	Met267 Leu197	Leu197	Met267 Leu197	Met267 Leu197	Ala268, Leu197 Leu197	Asp330, Lys219, Met267, Arg195 Leu197
Receptor tyrosine kinases								
								YW5
EGFR (8GB4)	Docking score (kcal mol^{-1})	−8.0287	−7.2188	−6.7622	−8.1569	−7.1292	−6.3271	−11.3781
	Types of interactions	3 H-bond Arene	4 H-bond	Arene	3 H-bond Arene	H-bond 3 Arene	Arene	3 H-bond Arene
	Residues	2 Met766, Asp855		Leu747		Glu749	Lie759	

Table 4 (*Contd.*)

Target enzyme (PDB)		6a	6b	6c	6e	6f	DOX	Co-crystalline ligand
		Lie759	Asp855, Met766, Phe856 Lys745		2 Met766, Asp855 Lie759	Phe723, Leu747, NME860		2 Asp855, Met766 Phe856
c-KIT (6GQJ)	Docking score (kcal mol^{-1})	−6.0324	−5.2508	−6.0765	−5.9900	−5.1218	−4.5458	**F82** −12.7068
	Types of interactions	H-bond	2 Arene	Arene	Arene	3 H-bond	H-bond	4 H-bond 2 Arene
	Residues	Cys637	Gly676, Leu595	Leu595	Leu595	Gly676, Cys673, Tyr672	Gly676	Glu671, Cys673, Asp810, Glu640 Leu595, Phe811
c-Met (3CD8)	Docking score (kcal mol^{-1})	−7.7871	−8.0868	−7.9845	−7.8021	−8.1638	−7.4166	**L5G** −9.5806
	Types of interactions	3 H-bond 3 Arene	3 H-bond 3 Arene	3 H-bond 2 Arene	H-bond 2 Arene	2 H-bond 3 Arene	2 H-bond 2 Arene	3 H-bond Arene
	Residues	Tyr1230, Arg1208, Arg1086 2 Tyr1230, Met1211	Tyr1230, Arg1208, Arg1086 2 Tyr1230, Lys1232	Tyr1230, Arg1208, Arg1086 Tyr1230, Lys1232	Arg1086 Tyr1230, Met1211	Arg1208, Arg1086 2 Tyr1230, Lys1232	Arg1208, Asn1167 2 Tyr1230	Arg1208, Asp1222, Met1160 Tyr1230
FGFR1 (4V01)	Docking score (kcal mol^{-1})	−7.3972	−7.4252	−7.4194	−7.7772	−7.8165	−6.9857	**0LI** −9.0744
	Types of interactions	H-bond	2 H-bond	2 H-bond	2 H-bond	2 H-bond	2 H-bond	3 H-bond 2 Arene
	Residues	Glu531	Glu531, Asp641	Glu531, Asp641	Glu531, Asp641	Glu531, Asp641	Cys619, Met535	Glu531, Asp641, His621 2 Leu484
Cyclin-dependent kinases (CDKs)								
CDK2 (2 A4L)	Docking score (kcal mol^{-1})	−6.4452	−6.9243	−7.1135	−6.8315	−6.9462	−7.1800	**RRC** −8.0278
	Types of interactions	2 H-bond 2 Arene	2 H-bond	3 H-bond Arene	H-bond Arene	2 H-bond	H-bond 2 Arene	2 H-bond
	Residues	Lys89, Leu83 Lys89, Lie10	Lys89, His84	Lys89, Leu83, His84 Lie10	Lys89 Lys89	Lys89, His84	Leu83 Phe80, Gly11	Glu81, Leu83
CDK4 (1GIH)	Docking score (kcal mol^{-1})	−8.0098	−7.5669	−7.6984	−8.8194	−8.0811	−8.1383	**1PU** −7.5254
	Types of interactions	H-bond Arene	2 Arene	4 Arene	H-bond Arene	4 Arene	2 H-bond Arene	3 H-bond

Table 4 (*Contd.*)

Target enzyme (PDB)		6a	6b	6c	6e	6f	DOX	Co-crystalline ligand
CDK6 (8I0M)	Residues	Leu83 Ala144	Gln131, Val18	2 Gln131, Glu12, Ala144	Leu83 Ala144	2 Gln131, Glu12, Ala144	Lie10, Glu12 Ala144	2 Leu83, Lys33 Val18
								NJ6
	Docking score (kcal mol^{-1})	−7.5315	−7.8884	−7.9575	−7.2575	−7.4880	−7.2081	−7.6397
	Types of interactions	Arene	2 Arene	2 Arene	H-bond Arene	Arene	3 H-bond	3 H-bond
	Residues	Phe164	Phe164, Glu21	Phe164, Glu21	Asp163 Glu21	Gln149	2 Val101, Asp104	Asp163, Glu99, Val101

2.3. Inverse-docking analysis

Protein tyrosine kinases (PTKs), which are divided into receptor and non-receptor tyrosine kinases, are essential enzymes that regulate vital cellular processes like growth, proliferation, and metabolism by transferring phosphate groups from ATP (adenosine triphosphate) to tyrosine residues on specific proteins within the cell.[35] Disruptions in this phosphorylation process can alter cell function and lead to various diseases, including cancer. PTK inhibitors, which block these enzymes and their uncontrolled signaling pathways, are a valuable foundation for developing new drug candidates. In recent years, the FDA has approved several kinase inhibitors for treating various cancers.[36] Additionally, cyclin-dependent kinases (CDKs) also play a crucial role by partnering with cyclins to phosphorylate target proteins and regulate cell cycle progression. In cancer, CDKs can become dysregulated through mutations or overexpression, resulting in unchecked cell proliferation. This loss of normal cell cycle regulation is a key factor in cancer development and progression.[37] Therefore, cyclin-dependent kinase inhibitors are useful therapeutic agents against many proliferative disorders, such as cancer.[38] Based on this understanding, the five most potent compounds, **6a–c**, **6e**, and **6f**, identified by the SRB assay as well as doxorubicin were subjected to an inverse-docking protocol to identify their potential targets. This technique involves docking a molecule against a library of potential target proteins to identify which proteins the ligand may bind to, thereby predicting its activity. The term "inverse" refers to identifying proteins that can accommodate a specific ligand, rather than finding ligands for a specific protein.[39–41] For this inverse docking protocol, a set of 12 proteins was used, including five non-receptor tyrosine kinases (ABL1, ABL2, PTK2, CDC42, PTK6), four receptor tyrosine kinases (EGFR, c-KIT, c-Met, FGFR1), and three cyclin-dependent kinases (CDK2, CDK4, CDK6) to perform comprehensive docking analysis against the five potent compounds.

The docking protocol was validated by redocking the co-crystallized ligand into the catalytic domain of the selected target proteins. Most of the redocked poses of the co-crystallized ligands maintained their binding conformations relative to the original poses, with an RMSD value of less than 1 Å. The 3D structures of the target proteins used for molecular docking were sourced from the Protein Data Bank (PDB). The binding energy and interactions for potent compounds are presented in Table 4, Fig. 6A–E, 7A–D and 8A–C while the interaction of doxorubicin with target protein are presented in "Supplementary File", Fig. 49. Based on the docking results for the selected non-receptor tyrosine kinase enzymes, the potent compounds showed good interactions with both ABL1 and ABL2, with comparable docking scores to the 1N1 ligand for ABL1, Fig. 6. In contrast, doxorubicin showed a lower binding score than both binding ligand and potent compounds, Table 4. For other selected enzymes such as PTK2 (PDB: 6I8Z), CDC42 (PDB: 3EQR), and PTK6 (PDB: 6CZ3), the docking scores were weaker compared to the co-crystallized ligands H82, T74, and FLJ, respectively, though PTK6 still demonstrated good binding

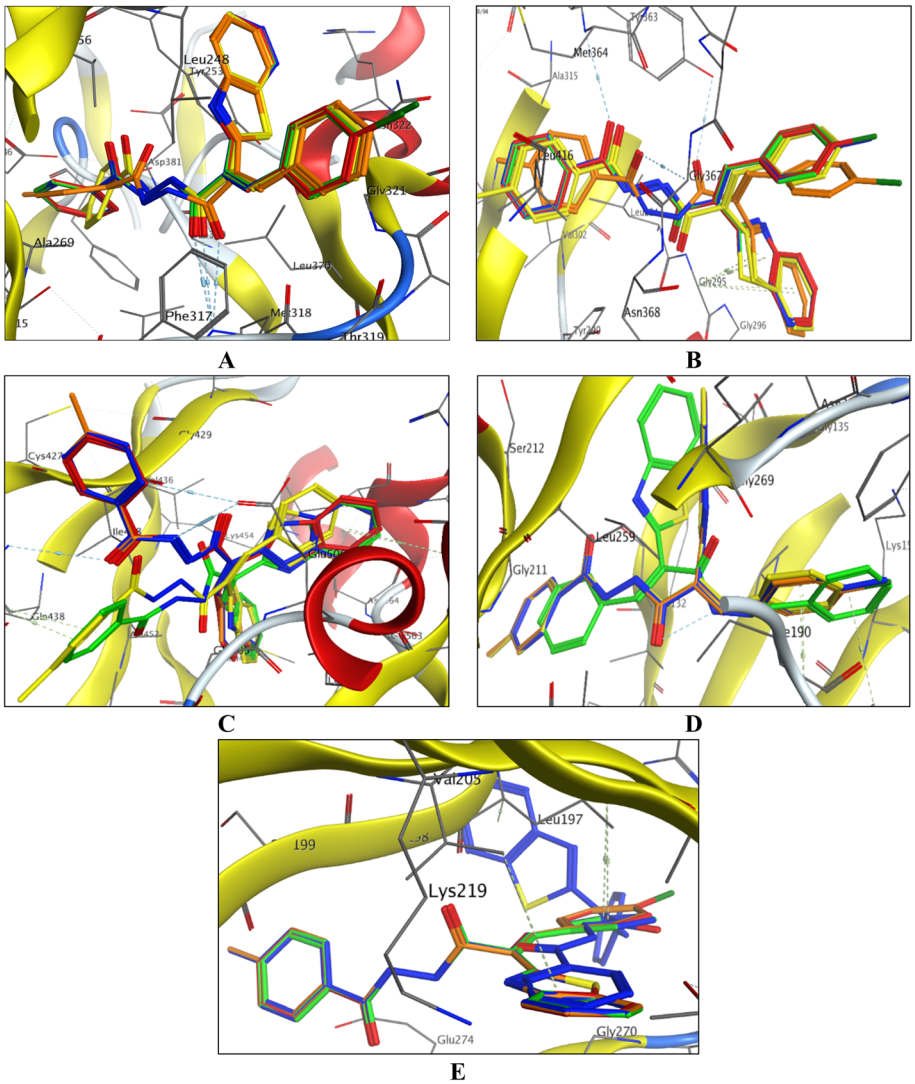

Fig. 6 3D interaction representation of **6a–c**, **6e** and **6f** compounds within the binding pocket of selected non-receptor tyrosine kinases enzymes. (A) ABL1, (B) ABL2, (C) PTK2, (D) CDC42, (E) PTK6. Compounds are color-coded as follows: **6a** (green), **6b** (red), **6c** (blue), **6e** (yellow), and **6f** (orange).

interactions, Table 4. The data indicated that for ABL1 (PDB: 2GQG), all compounds primarily formed hydrogen bonds with Met318, with additional arene interactions involving Asp381 for compounds **6e** and **6f**. This suggests strong interactions like the co-crystallized ligand 1N1. The docking scores ranged from −8.7770 to −8.6343 kcal mol^{-1}, compared to −9.2914 kcal mol^{-1} for 1N1. For ABL2 (PDB: 3HMI), the docked molecules maintained one hydrogen bond with Asp371 and arene interactions with Gly296 for all docked molecules, and extra one hydrogen bond with Met364 for compounds **6a–c**. The docking scores ranged from −6.0620 to −6.1636 kcal mol^{-1}, compared to −7.5292 kcal mol^{-1} for the co-crystallized ligand DKI. Despite the docking scores being lower than the co-crystallized ligand, the interaction patterns were still consistent and similar to those of the co-crystallized ligand DKI.

For the four selected receptor tyrosine kinase enzymes, the results indicated that all potent compounds as well as doxorubicin had lower docking scores compared to the co-crystallized ligands, Table 4 and Fig. 7A–D. Meanwhile, the potent compounds and doxorubicin showed comparable docking scores. For instance, in EGFR (PDB: 8GB4), the docking score of doxorubicin is −6.3271 kcal mol^{-1} and of the potent compounds ranged from −6.7622 kcal mol^{-1} to −8.1569 kcal mol^{-1}, whereas the co-crystallized ligand scored −11.3781 kcal mol^{-1}. Similarly, for c-KIT (PDB: 6GQJ), the scores of docked compounds **6a–c**, **6e** and **6f** ranged from −5.1218 kcal mol^{-1} to −6.0765 kcal mol^{-1}, with the co-crystallized ligand scoring −12.7068 kcal mol^{-1}, while maintaining consistent interaction patterns with key residues. In c-Met (PDB: 3CD8), the docked compounds showed several interactions with residues within the binding pocket. Compounds **6a–c** have three H-bond interactions with residues, Tyr1230, Arg1208, Arg1086, as well as arene interaction with Tyr1230 and Lys1232 residues. Additionally, for FGFR1 (PDB:

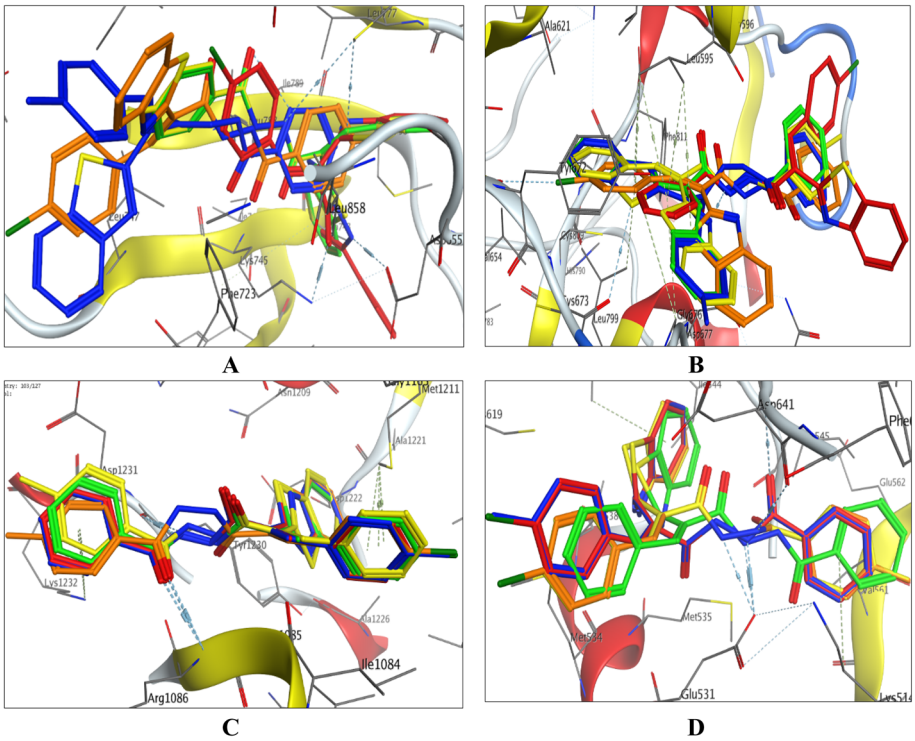

Fig. 7 3D interaction representation of **6a–c**, **6e** and **6f** compounds within the binding pocket of selected receptor tyrosine kinases enzymes. (A) EGFR, (B) c-Kit, (C) c-Met, (D) FGFR1. Compounds are color-coded as follows: **6a** (green), **6b** (red), **6c** (blue), **6e** (yellow), and **6f** (orange).

4V01), the docked compounds showed consistent interaction patterns involving Glu531 and Asp641 with lower docking scores compared to the co-crystallized ligand 0LI.

For cyclin-dependent kinases, Table 4 and Fig. 8A–C, the docking scores of doxorubicin and **6a–c**, **6e** and **6f** compounds for CDK4 (PDB: 1GIH) ranged from −7.5669 kcal mol^{-1} to

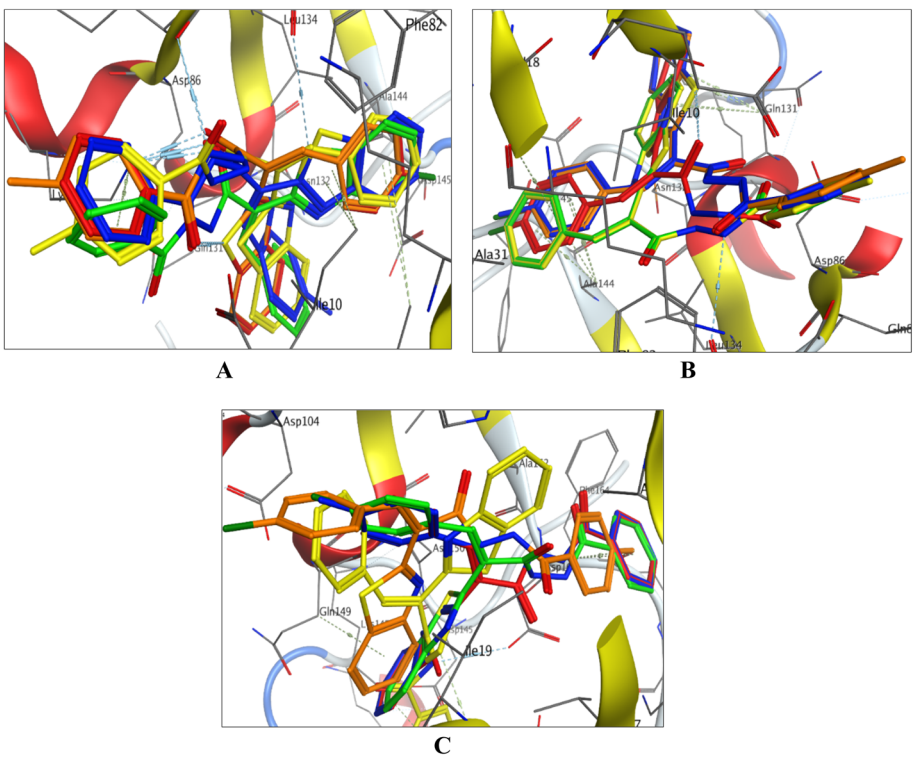

Fig. 8 3D interaction representation of **6a–c**, **6e** and **6f** compounds within the binding pocket of selected cyclin-dependent kinases enzymes. (A) CDK2, (B) CDK4, (C) CDK6. Compounds are color-coded as follows: **6a** (green), **6b** (red), **6c** (blue), **6e** (yellow), and **6f** (orange).

−8.8194 kcal mol^{-1}, slightly higher than the co-crystallized ligand 1PU, which scored −7.5254 kcal mol^{-1}. This result indicated strong binding potential like the co-crystallized ligand. For CDK6 (PDB: 8I0M), docking scores ranged from −7.2575 kcal mol^{-1} to −7.9575 kcal mol^{-1}, comparable to the co-crystallized ligand, which scored −7.6397 kcal mol^{-1}. Key interactions involved Phe164 and Glu21, suggesting these compounds could effectively inhibit CDK6. However, for CDK2 (PDB: 2A4L), the docked compounds showed lower docking scores, and different residue interactions compared to the co-crystallized ligand RRC.

Based on docking results, the five potent compounds have strong binding affinities to CDK4 and CDK6, suggesting that they can effectively inhibit these kinases. Since CDKs play a vital role in controlling the cell cycle, their inhibition would disrupt the cell cycle and potentially lead to the cessation of cell proliferation. This mechanism is consistent with the known effects of doxorubicin, which interferes with CDK activity and disrupts cell cycle regulation.[42] This highlights the potential of these compounds to be used as CDK inhibitors, contributing to their anti-cancer effects by halting cell cycle progression.

A future study will be conducted to investigate the *in vitro* and *in vivo* anti-proliferative effects of these compounds against CDK enzymes, comparing their efficacy to doxorubicin and assessing their potential for disrupting cell cycle progression.

3. Conclusions

In this study, a novel series of functionalized benzothiazole derivatives, including benzylidene and *N*-carboxamide 2-pyridone derivatives, was synthesized from *N*-aryl carboxohydrazides bearing a benzothiazole moiety. The anticancer activities of the newly synthesized compounds against three cell lines lung H1299, liver HEPG2 and breast cancers MCF7 revealed that five compounds **6a–c**, **6e**, and **6f** exhibited notable cytotoxicity against HepG2 and MCF7 cell lines, in some cases approaching the potency of the reference drug doxorubicin. According to the *in-silico* study, potent compounds demonstrated promising properties for drug development, including high GI absorption and selective CYP inhibition and exhibited promising characteristics for further investigation as potential drug candidates. The inverse-docking study demonstrated that the potent compounds exhibited consistent and significant interactions with key residues in both PTKs and CDKs, although with lower docking scores than the co-crystallized ligands. This indicates their potential as effective inhibitors, particularly for enzymes like ABL1, ABL2, CDK4, and CDK6.

To further elucidate the anticancer mode of action, future work will involve *in vitro* and *in vivo* mechanistic studies focusing on kinase inhibition, cell cycle arrest, and apoptotic pathways, thereby validating the predicted PTK/CDK interactions. Moreover, structural optimization will be explored through systematic variation of substituents on the benzylidene ring and by designing hybrid analogues incorporating alternative heterocycles to improve potency and selectivity. Together, these findings highlight the potential of benzothiazole derivatives as promising anticancer candidates and establish a foundation for targeted structural refinement and mechanistic validation in future studies.

4. Experimental section

4.1. Chemistry

All melting points were measured using a SMP3 melting point apparatus. IR spectra were recorded on an FTIR plus 460 or pyeunicam SP-1000 spectrophotometer using KBr pellets. The ^{1}H and ^{13}C NMR spectra were done in the Center of Drug Discovery Research and Development at Ain Shams University and recorded on a Bruker Avance (III)-400 Spectrometer (400 and 100 MHz, respectively) in DMSO-d_6 as a solvent using $Si(CH_3)_4$ as an internal standard and chemical shifts are reported as δ ppm units. Progress of the reactions was monitored by thin-layer chromatography (TLC) using aluminum sheets coated with silica gel F254 (Merck), and UV lamp.

Spectra of compounds **4b**, **4c**, **6f**, **6g**, **8c** and **10c** were set on the APT system (125 MHz) using a Bruker Advance (III)-500 MHz Spectrometer at Helwan University's Central Laboratory, Hub of Creativity and Scientific Research which produces even signals along with DMSO-d_6 signals.

4.2. General procedures for preparation compounds (4a–e)

A mixture of 2-(benzo[*d*]thiazol-2-yl)acetohydrazide **2** (0.08 mol) and pyridine (10 ml) were stirred for 15 min. Benzoyl chloride derivatives **3a–e** (0.16 mol) were added gradually to the reaction mixture in ice bath and stirred for 15 min. The reaction mixture was left at room temperature for 3 h. After the completion of the reaction, the solution was poured onto ice water and neutralized with HCl. The solid formed was filtered off and dried to produce a solid product. The solid product formed was washed using suitable solvent.

The preparation of compound *N*′-(2-(Benzo[*d*]thiazol-2-yl) acetyl)benzohydrazide (**4a**) has previously been described.[24]

4.2.1 *N*′-(2-(Benzo[*d*]thiazol-2-yl)acetyl)-4-chlorobenzohydrazide (4b). White solid, yield 80%, m.p: 225–226 °C; IR (KBr, cm^{-1}): ν 3264 (NH), 3033 (CH-Ar), 1683, 1655 (2CO); ^{1}H NMR (400 MHz, DMSO-d_6): δ 4.23 (s, 2H, CH_2), 7.44 (t, J = 7.8 Hz, 1H, benzothiazole-H), 7.51 (t, J = 6.6 Hz, 1H, benzothiazole-H), 7.58 (d, J = 10 Hz, 2H, Ar–H), 7.90 (d, J = 7.2 Hz, 2H, Ar–H), 7.98 (d, J = 8.4 Hz, 1H, benzothiazole-H), 8.09 (d, J = 10.8 Hz, 1H, benzothiazole-H), 10.60 (s, 2H, NH); ^{13}C-APT (125 MHz, DMSO-d_6): δ 39.3 (CH_2), 122.5, 122.7, 125.5, 126.5, 129.1, 129.9, 131.5, 135.8, 137.2, 152.6, 164.9 (11C, Ar–C), 165.9, 167.0 (2CO); anal. calcd for $C_{16}H_{12}ClN_3O_2S$ (345.80): C% 55.57; H% 3.50; N% 12.15; found: C% 55.60; H% 3.48; N% 12.13.

4.2.2 *N*′-(2-(Benzo[*d*]thiazol-2-yl)acetyl)-4-bromobenzohydrazide (4c). White solid, yield 80%, m.p: 238–239 °C; IR (KBr, cm^{-1}): ν 3265 (NH), 3033 (CH-Ar), 1683, 1656 (2CO); ^{1}H NMR (400 MHz, DMSO-d_6): δ 4.21 (s, 2H, CH_2), 7.44 (t, J = 7.2 Hz, 1H, benzothiazole-H), 7.51 (t, J = 7.4 Hz, 1H, benzothiazole-H), 7.73 (d, J = 8.4 Hz, 2H, Ar–H), 7.83 (d, J = 8.4 Hz, 2H, Ar–H), 7.97 (d, J = 8 Hz, 1H, benzothiazole-H), 8.09 (d, J = 7.2 Hz, 1H, benzothiazole-H), 10.49 (s, 1H, NH), 10.63 (s, 1H, NH); ^{13}C-APT (125 MHz, DMSO-d_6): δ 39.5 (CH_2), 122.5,

122.7, 125.5, 126.2, 126.5, 130.0, 131.8, 132.0, 135.8, 152.6, 164.9 (11C, Ar–C), 165.0, 167.0 (2CO); anal. calcd for $C_{16}H_{12}BrN_3O_2S$ (390.25): C% 49.24; H% 3.10; N% 10.77; found: C% 49.20; H% 3.13; N% 10.79.

4.2.3 *N′*-(2-(Benzo[*d*]thiazol-2-yl)acetyl)-4-methylbenzohydrazide (4d). White solid, yield 83%, m.p: 193–195 °C; IR (KBr, cm^{-1}): ν 3190 (NH), 3027 (CH-Ar), 1669, 1602 (2CO); ^{1}H NMR (400 MHz, DMSO-d_6): δ 2.36 (s, 3H, CH_3), 4.21 (s, 2H, CH_2), 7.30 (d, J = 8.0 Hz, 2H, Ar–H), 7.43 (t, J = 6.0 Hz, 1H, benzothiazole-H), 7.51 (t, J = 8.0 Hz, 1H, benzothiazole-H), 7.80 (d, J = 8.0 Hz, 2H, Ar–H), 7.98 (d, J = 8.0 Hz, 1H, benzothiazole-H), 8.08 (d, J = 8.0 Hz, 1H, benzothiazole-H), 10.45 (s, 1H, NH), 10.46 (s, 1H, NH); ^{13}C NMR (100 MHz, DMSO-d_6): δ 21.4 (CH_3), 39.4 (CH_2), 122.4, 122.7, 125.5, 126.5, 127.9, 129.5, 129.8, 135.7, 142.5, 152.6, 165.0 (11C, Ar–C), 165.9, 167.1 (2CO); anal. calcd for $C_{17}H_{15}N_3O_2S$ (325.38): C% 62.75; H% 4.65; N% 12.91; found: C% 62.78; H% 4.67; N% 12.89.

4.2.4 *N′*-(2-(Benzo[*d*]thiazol-2-yl)acetyl)-3-methoxybenzohydrazide (4e). White solid, yield 70%, m.p: 171–172 °C; IR (KBr, cm^{-1}): ν 3272 (NH), 3027 (CH-Ar), 1693, 1661 (2CO); ^{1}H NMR (400 MHz, DMSO-d_6): δ 3.81 (s, 3H, OCH_3), 4.20 (s, 2H, CH_2), 7.40 (d, J = 8.8 Hz, 1H, Ar–H), 7.39–7.53 (m, 5H, 3Ar–H & 2-benzothiazole-H), 7.98 (d, J = 8.8 Hz, 1H, benzothiazole-H), 8.09 (d, J = 10.8 Hz, 1H, benzothiazole-H), 10.46 (s, 1H, NH), 10.51 (s, 1H, NH); anal. calcd for $C_{17}H_{15}N_3O_3S$ (341.38): C% 59.81; H% 4.43; N% 12.31; found: C% 59.84; H% 4.40; N% 12.34.

4.3. General procedures for preparation compounds (6a–g)

A mixture of *N′*-(2-(benzo[*d*]thiazol-2-yl)acetyl)benzohydrazide derivatives **4a,d** (0.01 mol) and benzaldehyde derivatives **5a–d** (0.01 mol) were stirred at room temperature in ethanol containing a catalytic amount of piperidine (3 drops) for 5 h. After the completion of the reaction, the solution was poured onto ice water. The solid formed was filtered, dried, and washed using suitable solvent.

4.3.1 (*E*)-*N′*-(2-(Benzo[*d*]thiazol-2-yl)-3-phenylacryloyl) benzohydrazide (6a). Yellowish white solid, yield 75%, m.p: 216–217 °C; IR (KBr, cm^{-1}): ν 3267 (NH), 2993 (CH-Ar), 1641 (CO); ^{1}H NMR (400 MHz, DMSO-d_6): δ 7.45–7.58 (m, 7H, 6 Ar–H & 1-benzothiazole-H), 7.62 (t, J = 6.6 Hz, 1H, benzothiazole-H), 7.75 (s, 1H, CH), 7.97–8.04 (m, 5H, 4Ar–H & 1-benzothiazole-H), 8.15 (d, J = 8.4 Hz, 1H, benzothiazole-H), 10.73 (s, 1H, NH), 10.89 (s, 1H, NH); anal. calcd for $C_{23}H_{17}N_3O_2S$ (399.46): C% 69.15; H% 4.29; N% 10.52; found: C% 69.19; H% 4.28; N% 10.50.

4.3.2 (*E*)-*N′*-(2-(Benzo[*d*]thiazol-2-yl)-3-(4-chlorophenyl) acryloyl)benzohydrazide (6b). Yellowish white solid, yield 75%, m.p: 232–233 °C; IR (KBr, cm^{-1}): ν 3268 (NH), 2923 (CH-Ar), 1692, 1644 (2CO); ^{1}H NMR (400 MHz, DMSO-d_6): δ 7.47–7.62 (m, 7H, 6 Ar–H & 1-benzothiazole-H), 7.75 (s, 1H, CH), 7.98–8.04 (m, 5H, 4Ar–H & 1-benzothiazole-H), 8.15 (d, J = 8.4 Hz, 1H, benzothiazole-H), 10.70 (s, 2H, NH); ^{13}C NMR (100 MHz, DMSO-d_6): δ 122.6, 123.2, 126.4, 127.2, 128.1, 128.9, 129.1, 130.9, 132.4, 132.5, 132.8, 132.8, 134.5, 134.8, 134.9, 153.4, 165.5 (Ar–C), 166.2, 166.4 (2CO); anal. calcd for $C_{23}H_{16}ClN_3O_2S$ (433.91): C% 63.66; H% 3.72; N% 9.68; found: C% 63.69; H% 3.70; N% 9.72.

4.3.3 (*E*)-*N′*-(2-(Benzo[*d*]thiazol-2-yl)-3-(*p*-tolyl)acryloyl)benzohydrazide (6c). Yellowish white solid, yield 73%, m.p: 232–233 °C; IR (KBr, cm^{-1}): ν 3269 (NH), 2921 (CH-Ar), 1686, 1643 (2CO); ^{1}H NMR (400 MHz, DMSO-d_6): δ 2.37 (s, 3H, CH_3), 7.27 (d, J = 6.4 Hz, 2H, Ar–H), 7.47 (t, J = 7.6 Hz, 1H, benzothiazole-H), 7.53–7.57 (m, 3H, Ar–H), 7.62 (t, J = 7.0 Hz, 1H, benzothiazole-H), 7.70 (s, 1H, CH), 7.88 (d, J = 7.6 Hz, 2H, Ar–H), 7.99–8.02 (m, 3H, 2Ar–H & benzothiazole-H), 8.14 (d, J = 8.0 Hz, 1H, benzothiazole-H), 10.72 (s, 1H, NH), 10.82 (s, 1H, NH); anal. calcd for $C_{24}H_{19}N_3O_2S$ (413.50): C% 69.71; H% 4.63; N% 10.16; found: C% 69.74; H% 4.60; N% 10.15.

4.3.4 (*E*)-*N′*-(2-(Benzo[*d*]thiazol-2-yl)-3-(4-methoxyphenyl) acryloyl)benzohydrazide (6d). Yellow solid, yield 73%, m.p: 215–217 °C; IR (KBr, cm^{-1}): ν 3270 (NH), 2924 (CH-Ar), 1685, 1645 (CO); ^{1}H NMR (400 MHz, DMSO-d_6): δ 3.82 (s, 3H, OCH_3), 7.00 (d, J = 7.6 Hz, 2H, Ar–H), 7.46 (t, J = 8.0 Hz, 1H, benzothiazole-H), 7.52–7.57 (m, 3H, Ar–H), 7.62 (t, J = 7.6 Hz, 1H, benzothiazole-H), 7.67 (s, 1H, CH), 7.95–8.01 (m, 5H, 4Ar–H & 1-benzothiazole-H), 8.12 (d, J = 8 Hz, 1H, benzothiazole-H), 10.70 (s, 1H, NH), 10.81 (s, 1H, NH); ^{13}C NMR (100 MHz, DMSO-d_6):δ 55.8 (OCH_3), 114.6, 122.5, 122.9, 125.8, 126.4, 127.0, 127.8, 128.2, 128.9, 132.3, 132.9, 133.0, 134.7, 135.8, 153.6, 161.1, 165.9 (17C, Ar–C), 166.3, 166.9 (2CO); anal. calcd for $C_{24}H_{19}N_3O_3S$ (429.11): C% 67.12; H% 4.46; N% 9.78; found: C% 67.16; H% 4.49; N% 9.74.

4.3.5 (*E*)-*N′*-(2-(Benzo[*d*]thiazol-2-yl)-3-phenylacryloyl)-4-methylbenzohydrazide (6e). White solid, yield 65%, m.p: 200–203 °C; IR (KBr, cm^{-1}): ν 3265 (NH), 2971 (CH-Ar), 1684, 1641 (2CO); ^{1}H NMR (400 MHz, DMSO-d_6): δ 2.40 (s, 3H, CH_3), 7.35 (d, J = 8.0 Hz, 2H, Ar–H), 7.44–7.50 (m, 4H, Ar–H & benzothiazole-H), 7.56 (t, J = 7.2 Hz, 1H, benzothiazole-H), 7.74 (s, 1H, CH), 7.90 (d, J = 7.6 Hz, 2H, Ar–H), 7.97–7.99 (m, 2H, Ar–H), 8.02 (d, J = 8.0 Hz, 1H, benzothiazole-H), 8.15 (d, J = 8.4, 1H, benzothiazole-H), 10.71 (s, 2H, NH); anal. calcd for $C_{24}H_{19}N_3O_2S$ (413.49): C% 69.71; H% 4.63; N% 10.16; found: C% 69.75; H% 4.65; N% 10.13.

4.3.6 (*E*)-*N′*-(2-(Benzo[*d*]thiazol-2-yl)-3-(4-chlorophenyl) acryloyl)-4-methylbenzohydrazide (6f). White solid, yield 75%, m.p: 223–224 °C; IR (KBr, cm^{-1}): ν 3269 (NH), 2923 (CH-Ar), 1686,1645 (CO); ^{1}H NMR (400 MHz, DMSO-d_6): δ 2.40 (s, 3H, CH_3), 7.35 (d, J = 8.0 Hz, 2H, Ar–H), 7.47–7.50 (m, 3H, 2Ar–H & 1-benzothiazole-H), 7.56 (t, J = 7.8 Hz, 1H, benzothiazole-H), 7.75 (s, 1H, CH), 7.90 (d, J = 8.4 Hz, 2H, Ar–H), 8.00–8.04 (m, 3H, 2Ar–H & 1-benzothiazole-H), 8.15 (d, J = 8.4 Hz, 1H, benzothiazole-H), 10.73 (s, 2H, NH); ^{13}C-APT (125 MHz, DMSO-d_6): δ 21.5 (CH_3), 122.6, 123.2, 126.2, 127.2, 128.2, 129.1, 129.5, 130.1, 131.0, 132.5, 132.8, 134.8, 135.0, 142.4, 153.5, 165.5 (17C, Ar–C), 166.2, 166.3 (2CO); anal. calcd for $C_{24}H_{18}ClN_3O_2S$ (447.94): C% 64.35; H% 4.05; N% 9.38; found: C% 64.34; H% 4.06; N% 9.36.

4.3.7 (*E*)-*N′*-(2-(Benzo[*d*]thiazol-2-yl)-3-(4-methoxyphenyl) acryloyl)-4-methylbenzohydrazide (6g). Off white solid, yield 75%, m.p: 241–243 °C; IR (KBr, cm^{-1}): ν 3278 (NH), 2953 (CH-Ar), 1681, 1636 (2CO); ^{1}H NMR (400 MHz, DMSO-d_6): δ 2.39 (s, 3H, CH_3), 3.86 (s, 3H, OCH_3), 6.99 (d, J = 9.2 Hz, 2H, Ar–H), 7.35

(d, J = 13.6 Hz, 2H, Ar–H), 7.45 (t, J = 11.6 Hz, 1H, benzothiazole-H), 7.54 (t, J = 9.8 Hz, 1H, benzothiazole-H), 7.69 (s, 1H, CH), 7.93 (d, J = 11.6 Hz, 2H, Ar–H), 7.97–8.02 (m, 3H, 2Ar–H & benzothiazole-H), 8.12 (d, J = 9.0 Hz, 1H, benzothiazole-H), 10.64 (s, 1H, NH), 10.77 (s, 1H, NH); ^{13}C-APT (125 MHz, DMSO-d_6): δ 21.5 (CH_3), 55.8 (OCH_3), 114.6, 122.5, 122.9, 125.8, 126.5, 127.0, 127.9, 128.2, 129.5, 130.2, 132.9, 134.8, 135.7, 142.3, 153.6, 161.1, 165.9 (17C, Ar–C), 166.2, 166.9 (2CO); anal. calcd for $C_{25}H_{21}N_3O_3S$ (443.52): C% 67.70; H% 4.77; N% 9.47; found: C% 67.73; H% 4.75; N% 9.44.

4.4. General procedures for preparation of compounds (8a–c)

A mixture of *N*′-(2-(benzo[*d*]thiazol-2-yl)acetyl)benzohydrazide derivatives **4a,d** (0.01 mole) and 2-(ethoxymethylene)malononitrile **7a** or (*E*)-ethyl 2-cyano-3-ethoxyacrylate **7b** (0.017 mole) were refluxed in ethanol (30 ml) containing sodium ethoxide (0.01 mole) for 5 hours. The formed precipitate was filtered then washed using suitable solvent after drying.

4.4.1 *N*-(6-Amino-3-(benzo[*d*]thiazol-2-yl)-5-cyano-2-oxopyridin-1(2*H*)-yl)benzamide (8a). Orange solid, yield 70%, m.p: over 350 °C; IR (KBr, cm^{-1}): ν 3430 (NH, NH_2), 2924 (CH-Ar), 2216 (CN), 1631 (CO); ^{1}H NMR (400 MHz, DMSO-d_6): δ 7.30 (t, J = 9.8 Hz, 1H, benzothiazole-H), 7.45 (t, J = 8.4 Hz, 1H, benzothiazole-H), 7.50–7.56 (m, 3H, 3Ar–H), 7.89 (d, J = 8.4 Hz, 1H, benzothiazole-H), 8.04 (d, J = 7.6 Hz, 1H, benzothiazole-H), 8.23 (d, J = 7.2 Hz, 2H, Ar–H), 8.73 (s, 1H, pyridone-H); ^{13}C NMR (100 MHz, DMSO-d_6): δ 118.6 (CN), 76.7, 103.9, 121.2, 122.0, 123.6, 126.1, 127.2, 129.2, 130.2, 131.4, 135.0, 136.8, 152.4, 153.7, 156.4 (15C, Ar–C), 162.1, 164.1 (2CO); anal. calcd for $C_{20}H_{13}N_5O_2S$ (387.41): C% 62.00; H% 3.38; N% 18.08; found: C% 62.02; H% 3.40; N% 18.06.

4.4.2 Ethyl 2-amino-1-benzamido-5-(benzo[*d*]thiazol-2-yl)-6-oxo-1,6-dihydropyridine-3-carboxylate (8b). Orange solid, yield 65%, m.p: over 350 °C; IR (KBr, cm^{-1}): ν 3433 (NH, NH_2), 2925 (CH-Ar), 1685, 1614 (2CO); ^{1}H NMR (400 MHz, DMSO-d_6): δ 1.40 (t, J = 7.1 Hz, 3H, CH_3), 4.36 (q, J = 7.1 Hz, 2H, CH_2), 7.29 (t, J = 7.6 Hz, 1H, benzothiazole-H), 7.42–7.56 (m, 4H, 3Ar–H & 1benzothiazole-H), 7.91 (d, J = 8.1 Hz, 1H, benzothiazole-H), 8.02 (d, J = 7.8 Hz, 1H, benzothiazole-H), 8.26 (d, J = 7.4 Hz, 2H, Ar–H), 9.15 (s, 1H, pyridone-H); anal. calcd for $C_{22}H_{18}N_4O_4S$ (434.47): C% 60.82; H% 4.18; N% 12.90; found: C% 60.83; H% 4.20; N% 12.91.

4.4.3 Ethyl 2-amino-5-(benzo[*d*]thiazol-2-yl)-1-(4-methylbenzamido)-6-oxo-1,6-dihydropyridine-3-carboxylate (8c). Orange solid, yield 65%, m.p: over 350 °C; IR (KBr, cm^{-1}): ν 3433 (NH, NH_2), 2920 (CH-Ar), 1685, 1614 (2CO); ^{1}H NMR (400 MHz, DMSO-d_6): δ 1.39 (t, J = 7.4 Hz, 3H, CH_3), 2.44 (s, 3H, CH_3), 4.38 (q, J = 7.0 Hz, 2H, CH_2), 7.34 (t, J = 8.8 Hz, 1H, benzothiazole-H), 7.42 (d, J = 12.0 Hz, 2H, Ar–H), 7.48 (t, J = 8.8 Hz, 1H, benzothiazole-H), 7.95–8.00 (m, 3H, 2Ar–H & 1-benzothiazole-H), 8.04 (d, J = 8.0 Hz, 1H, benzothiazole-H), 8.86 (s, 2H, NH_2), 9.12 (s, 1H, pyridone-H), 11.05 (s, 1H, NH); ^{13}C-APT (125 MHz, DMSO-d_6): δ 14.9, 21.6 (2CH_3), 61.1 (CH_2), 89.8, 106.6, 121.8, 122.2, 124.4, 126.5, 128.8, 129.1, 129.4, 135.1, 140.3, 143.3, 152.3, 157.2, 158.4 (15C, Ar–C), 162.5, 166.3, 166.9 (3CO); anal. calcd for $C_{23}H_{20}N_4O_4S$ (448.49): C% 61.59; H% 4.49; N% 12.49; found: C% 61.61; H% 4.47; N% 12.47.

4.5. General procedures for preparation of compounds (10a–c)

A mixture of *N*′-(2-(benzo[*d*]thiazol-2-yl)acetyl)benzohydrazide derivatives **4a,d** (0.01 mole) and (*Z*)-2-cyano-3-(dimethylamino)-*N*-arylacrylamide derivatives **9a–c** (0.01 mol) were refluxed in dioxane containing equimolar of KOH (0.01 mol) for 7 hours. The precipitate formed was filtered then after drying it was washed using a suitable solvent.

4.5.1 2-Amino-1-benzamido-5-(benzo[*d*]thiazol-2-yl)-6-oxo-*N*-phenyl-1,6-dihydropyridine-3-carboxamide (10a). Offwhite solid, yield 65%, m.p: over 350 °C; IR (KBr, cm^{-1}): ν 3430, 3328 (NH, NH_2), 2938 (CH-Ar), 1631 (CO); ^{1}H NMR (400 MHz, DMSO-d_6): δ 7.12 (t, J = 7.0 Hz, 1H, benzothiazole-H), 7.29 (t, J = 7.0 Hz, 1H, benzothiazole-H), 7.44–7.61 (m, 6H, Ar–H), 7.86–7.93 (m, 3H, 2Ar–H & 1-benzothiazole-H), 8.03 (d, J = 7.6 Hz, 1H, benzothiazole-H), 8.32 (d, J = 8.0 Hz, 2H, Ar–H), 9.25 (s, 1H, pyridone-H), 11.60 (s, 1H, NH); anal. calcd for $C_{26}H_{19}N_5O_3S$ (481.53): C% 64.85; H% 3.98; N% 14.54; found: C% 64.87; H% 3.97; N% 14.53.

4.5.2 2-Amino-5-(benzo[*d*]thiazol-2-yl)-*N*-(4-chlorophenyl)-1-(4-methylbenzamido)-6-oxo-1,6-dihydropyridine-3-carboxamide (10b). Offwhite solid, yield 73%, m.p: over 350 °C; IR (KBr, cm^{-1}): ν 3489, 3224 (NH, NH_2), 2916 (CH-Ar), 1660, 1614 (2CO); ^{1}H NMR (400 MHz, DMSO-d_6): δ 2.42 (s, 3H, CH_3), 7.30 (t, J = 10.4 Hz, 1H, benzothiazole-H), 7.40–7.49 (m, 5H, 4Ar–H & 1-benzothiazole-H), 7.89–7.94 (m, 3H, 2Ar–H & 1-benzothiazole-H), 8.03 (d, J = 9.6 Hz, 1H, benzothiazole-H), 8.20 (d, J = 14.0 Hz, 2H, Ar–H), 9.23 (s, 1H, pyridone-H), 11.68 (s, 1H, NH); ^{13}C NMR (100 MHz, DMSO-d_6): δ 21.5 (CH_3), 98.9, 103.9, 121.1, 121.9, 123.3, 125.9, 126.8, 127.2, 128.4, 129.4, 129.9, 134.4, 135.2, 138.9, 139.9, 152.7, 156.6 (17C, Ar–C), 160.7, 162.5, 165.0 (3CO); anal. calcd for $C_{27}H_{20}ClN_5O_3S$ (530.00): C% 61.19; H% 3.80; N% 13.21; found: C% 61.22; H% 3.84; N% 13.20.

4.5.3 2-Amino-5-(benzo[*d*]thiazol-2-yl)-1-(4-methylbenzamido)-6-oxo-*N*-(*p*-tolyl)-1,6-dihydropyridine-3-carboxamide (14c). Beige solid, yield 62%, m.p: over 350 °C; IR (KBr, cm^{-1}): ν 3500, 3330 (NH, NH_2), 2915 (CH-Ar), 1624, 1610 (2CO); ^{1}H NMR (400 MHz, DMSO-d_6): δ 2.32 (s, 3H, CH_3), 2.42 (s, 3H, CH_3), 7.23 (d, J = 8.4 Hz, 2H, Ar–H), 7.29 (t, J = 7.6 Hz, 1H, benzothiazole-H), 7.40–7.46 (m, 3H, 2Ar–H & benzothiazole-H), 7.74 (d, J = 9.2 Hz, 2H, Ar–H), 7.92 (d, J = 7.6 Hz, 1H, benzothiazole-H), 8.02 (d, J = 6.0 Hz, 1H, benzothiazole-H), 8.19 (d, J = 8.0 Hz, 2H, Ar–H), 9.23 (s, 1H, pyridone-H), 11.54 (s, 1H, NH); ^{13}C-APT (125 MHz, DMSO-d_6): δ 20.9, 21.5 (2CH_3), 99.4, 103.7, 119.5, 121.1, 121.9, 123.3, 125.9, 127.2, 128.5, 129.9, 130.0, 132.3, 134.3, 135.3, 137.5, 139.9, 152.7, 152.8, 156.6 (19C, Ar–C), 160.6, 162.2, 165.2 (3CO); anal. calcd for $C_{28}H_{23}N_5O_3S$ (509.15): C% 66.00; H% 4.55; N% 13.74; found: C% 66.02; H% 4.53; N% 13.72.

4.6. Anticancer activity

Human tumor carcinoma cell lines (H1299- HEPG2- MCF7) were used in this study were obtained from the American Type

Culture Collection (ATCC, Minisota, U.S.A.). The tumor cell lines were maintained at the National Cancer Institute, Cairo, Egypt, by serial sub-culturing. Samples were prepared by dissolving 1 : 1 Stock solution and stored at −20 °C in DMSO at 100 mM. Different concentrations of the drug were used 0.00, 6.25, 12.5, 25, 50 μg ml^{-1}.

The cytotoxicity was carried out using SRB (used as a protein dye) assay.[43] Cells were seeded in 96-well microtiter plates at initial concentration of 3×10^3 cell per well in a 150 μl fresh medium and left for 24 h for attachment. Different concentrations 0, 6.25, 12.5, 25, 50 μg ml^{-1} of drug were added in triplicate for each drug concentration. The plates were incubated for 48 h at 37 °C, 5% CO_2. By the end of incubation, cells were fixed with 50 μl cold trichloroacetic acid 10% final concentration for 1 h at 4 °C. The plates were washed with distilled water using (automatic washer Tecan, Germany) and stained with 50 μl 0.4% SRB dissolved in 1% acetic acid for 30 minutes at room temperature. The plates were washed four times with 1% acetic acid and air-dried, followed by addition of 200 ml 10 mM Tris base solution (pH 10.5) to each well and shake the plate on a gyratory shaker for 5 min to solubilize the protein-bound dye. Optical density (O.D.) of each well was measured spectrophoto metrically at 570 nm with an ELISA microplate reader (Sunrise Tecan reader, Germany). The mean background absorbance was automatically subtracted and mean values of each drug concentration were calculated. The experiment was repeated 3 times. The percentage of cell survival was calculated after subtraction of background blank O.D. as follows:

Surviving fraction = O.D. (treated cells)/O.D. (untreated cells).

The IC_{50} values (the concentrations of drug required to produce 50% inhibition of cell growth) were also calculated using GraphPad Prism 8.

4.7. *In silico* ADME study

Drug-likeness is a qualitative notion in drug design that predicts a drug-like feature. Therapeutic-like qualities such as solubility, permeability, transporter effects, and metabolic stability are essential for therapeutic candidates' success. They have an influence on oral bioavailability, toxicity, metabolism, clearance, and *in vitro* pharmacology. The drug-likeness of the synthesized compounds was evaluated using five independent filters, including the Lipinski,[44] Ghose,[45] Muegge,[46] Veber,[47] and Egan[48] guidelines, as well as bioavailability and drug-likeness scores using the Swiss ADME program.

4.8. Pass analysis

The PASS system provides users with a list of expected activity forms in addition to estimates of the likelihood that each type of activity is either active (Pa) or inactive (Pi), measured on a range of 0 to 1. These probabilities are used as markers of the compound's possible membership in imprecise categories of chemical compounds that are either active or inactive. Based on these probabilities, various criteria can be developed to evaluate prediction results pertinent to real-world problems. The PASS program's efficacy has been demonstrated in a variety of domains, including the identification of compounds with multitarget action against hypertension and inflammation, the discovery of novel biological activities for medically used drugs, and the evaluation of pharmaceutical side effects and toxicity mechanisms. This computer-based software, available through an online platform called PASS (Prediction of Probable Activity Spectra of Substances) analysis (**https://www.pharmaexpert.ru/passonline**), allows for the examination of a compound's biological and pharmacological potential, as well as the elucidation of its interactions with other biological entities. The PASS application accepts data in the Mol file format for individual structures or the SDF file format for collections of structures.

4.9. Molecular docking study

All the invers docking analysis was conducted using the Molecular Operating Environment (MOE 2014). The ligand molecules were pulled by the building molecules, and their energy was reduced. All minimizations were performed until the MMFF94X force field achieved an RMSD gradient of 0.01 kcal mol^{-1}, at which point the partial charges were calculated automatically. Docking simulations were carried out utilizing the Protein Data Bank's crystal structure of twelve enzymes, ABL1, ABL2, PTK2, CDC42, PTK6, EGFR, c-KIT, c-Met, FGFR1, CDK2, CDK4, and CDK6, in association with co-crystallin ligand 1N1, DKI, H82, T74, FLJ, YW5, F82, L5G, 0LI, RRC, 1PU, and NJ6 (PDB ID: 2GQG, 3HMI, 6I8Z, 3EQR, 6CZ3, 8GB4, 6GQJ, 3CD8, 4V01, 2 A4L, 1GIH, and 8I0M). The MOE protonate 3D application was used to add the missing hydrogens and assign the right ionization states. The MOE-Alpha site finder was used to create an active site. Re-docking the co-crystallized ligands into their respective protein binding sites was performed. The reproduced poses were in close agreement with the experimental conformations, with root mean square deviation (RMSD) values of less than 2.0 Å, confirming the validity of the docking procedure. Ligands were then docked within the active sites using the MOE-Dock. The GBVI/WSA DG free-energy estimates were used to rank the optimized poses and docking poses were examined visually. The interactions with binding pocket residues were finally investigated.

Author contributions

Conceptualization: GHE, RAA; methodology: GHE, RAA, MMS, MAE; writing-original draft preparation: GHE, RAA; writing-review and editing: GHE, RAA and MAE.

Conflicts of interest

The authors have no conflicts of interest to declare.

Data availability

The datasets generated during and/or analyzed during the current study are available from the corresponding author.

Supplementary information is available. See DOI: https://doi.org/10.1039/d5ra03277f.

Acknowledgements

The authors express their gratitude to the Central Laboratory of Helwan University (CLHU) at the headquarters of the Centers of Excellence and Scientific Innovation at Helwan University for conducting ^{13}C-APT analysis.

References

1 H.-Y. Lin and J. Y. Park, in *Anesthesia for Oncological Surgery*, Springer International Publishing, Cham, 2023, pp. 11–16.
2 J. Ferlay, M. Colombet, I. Soerjomataram, D. M. Parkin, M. Piñeros, A. Znaor and F. Bray, *Int. J. Cancer*, 2021, **149**, 778–789.
3 C. Allemani, H. K. Weir, H. Carreira, R. Harewood, D. Spika, X.-S. Wang, F. Bannon, J. V Ahn, C. J. Johnson, A. Bonaventure, R. Marcos-Gragera, C. Stiller, G. Azevedo e Silva, W.-Q. Chen, O. J. Ogunbiyi, B. Rachet, M. J. Soeberg, H. You, T. Matsuda, M. Bielska-Lasota, H. Storm, T. C. Tucker and M. P. Coleman, *Lancet*, 2015, **385**, 977–1010.
4 E. Morgan, M. Arnold, A. Gini, V. Lorenzoni, C. J. Cabasag, M. Laversanne, J. Vignat, J. Ferlay, N. Murphy and F. Bray, *Gut*, 2023, **72**, 338–344.
5 S. Lin, C. Liu, X. Zhao, X. Han, X. Li, Y. Ye and Z. Li, *Front. Chem.*, 2022, **10**, 869860.
6 M. Alrooqi, S. Khan, F. A. Alhumaydhi, S. A. Asiri, M. Alshamrani, M. M. Mashraqi, A. Alzamami, A. M. Alshahrani and A. A. Aldahish, *Anticancer Agents Med. Chem.*, 2022, **22**, 2775–2787.
7 A. Kamal, M. A. H. Syed and S. M. Mohammed, *Expert Opin. Ther. Pat.*, 2015, **25**, 335–349.
8 N. Pathak, E. Rathi, N. Kumar, S. G. Kini and C. M. Rao, *Mini-Rev. Med. Chem.*, 2020, **20**, 12–23.
9 T. Bradshaw, S. Wrigley, D.-F. Shi, R. Schultz, K. Paull and M. Stevens, *Br. J. Cancer*, 1998, **77**, 745–752.
10 B. S. Tan, K. H. Tiong, A. Muruhadas, N. Randhawa, H. L. Choo, T. D. Bradshaw, M. F. G. Stevens and C.-O. Leong, *Mol. Cancer Ther.*, 2011, **10**, 1982–1992.
11 T. Bradshaw, M. F. Stevens and A. Westwell, *Curr. Med. Chem.*, 2001, **8**, 203–210.
12 R. S. Keri, M. R. Patil, S. A. Patil and S. Budagumpi, *Eur. J. Med. Chem.*, 2015, **89**, 207–251.
13 T. I. Ismail, N. El-Khazragy and R. A. Azzam, *RSC Adv.*, 2024, **14**, 16332–16348.
14 A. Irfan, F. Batool, S. A. Zahra Naqvi, A. Islam, S. M. Osman, A. Nocentini, S. A. Alissa and C. T. Supuran, *J. Enzyme Inhib. Med. Chem.*, 2020, **35**, 265–279.
15 X. Xu, Z. Zhu, S. Chen, Y. Fu, J. Zhang, Y. Guo, Z. Xu, Y. Xi, X. Wang, F. Ye, H. Chen and X. Yang, *Front. Chem.*, 2024, **12**, 1384301.
16 M. Kim, M. Baek and D. J. Kim, *Curr. Pharm. Des.*, 2017, **23**, 4226–4246.
17 M. S. Ebaid, H. A. Abdelsattar Ibrahim, A. F. Kassem and A. Sabt, *RSC Adv.*, 2024, **14**, 36989–37018.
18 H. A. Bhuva and S. G. Kini, *J. Mol. Graphics Modell.*, 2010, **29**, 32–37.
19 A. K. El-Damasy, H. Jin, J. W. Park, H. J. Kim, H. Khojah, S. H. Seo, J.-H. Lee, E.-K. Bang and G. Keum, *J. Enzyme Inhib. Med. Chem.*, 2023, **38**, 2189097.
20 Y. Zhang and A. Pike, *Bioorg. Med. Chem. Lett.*, 2021, **38**, 127849.
21 R. C. Pandey, M. W. Toussaint, R. M. Stroshane, C. C. Kalita, A. A. Aszalos, A. L. Garretson, T. T. Wei, K. M. Byrne, R. M. Stroshane and R. J. White, *J. Antibiot.*, 1981, **34**, 1389–1401.
22 V. J. Venditto and E. E. Simanek, *Mol. Pharm.*, 2010, **7**, 307–349.
23 R. A. Azzam, G. H. Elgemeie, R. E. Elsayed and P. G. Jones, *Acta Crystallogr., Sect. E:Crystallogr. Commun.*, 2017, **73**, 1041–1043.
24 R. A. Azzam, G. H. Elgemeie, M. M. Seif and P. G. Jones, *Acta Crystallogr., Sect. E:Crystallogr. Commun.*, 2021, **77**, 891–894.
25 M. A. Khedr, W. A. Zaghary, G. E. Elsherif, R. A. Azzam and G. H. Elgemeie, *Nucleosides, Nucleotides Nucleic Acids*, 2023, **42**, 77–104.
26 R. A. Azzam, G. H. Elgemeie, R. R. Osman and P. G. Jones, *Acta Crystallogr., Sect. E:Crystallogr. Commun.*, 2019, **75**, 367–371.
27 R. A. Azzam, G. H. Elgemeie, R. E. Elsayed and P. G. Jones, *Acta Crystallogr., Sect. E:Crystallogr. Commun.*, 2017, **73**, 1041–1043.
28 R. A. Azzam, R. E. Elsayed and G. H. Elgemeie, *ACS Omega*, 2020, **5**, 10401–10414.
29 R. A. Azzam, H. A. Elboshi and G. H. Elgemeie, *Antibiotics*, 2022, **11**, 1799.
30 R. E. Elsayed, T. M. Madkour and R. A. Azzam, *Int. J. Biol. Macromol.*, 2020, **164**, 1984–1999.
31 R. A. Azzam, H. A. Elboshi and G. H. Elgemeie, *ACS Omega*, 2020, **5**, 30023–30036.
32 R. A. Azzam, R. E. Elsayed and G. H. Elgemeie, *ACS Omega*, 2020, **5**, 26182–26194.
33 R. A. Azzam, G. H. Elgemeie and R. R. Osman, *J. Mol. Struct.*, 2020, **1201**, 127194.
34 R. A. Azzam, N. M. Gad and G. H. Elgemeie, *ACS Omega*, 2022, **7**, 35656–35667.
35 S. R. Hubbard and J. H. Till, *Annu. Rev. Biochem.*, 2000, **69**, 373–398.
36 P. Wu, T. E. Nielsen and M. H. Clausen, *Drug Discovery Today*, 2016, **21**, 5–10.
37 U. Asghar, A. K. Witkiewicz, N. C. Turner and E. S. Knudsen, *Nat. Rev. Drug Discovery*, 2015, **14**, 130–146.
38 S. Ghafouri-Fard, T. Khoshbakht, B. M. Hussen, P. Dong, N. Gassler, M. Taheri, A. Baniahmad and N. A. Dilmaghani, *Cancer Cell Int.*, 2022, **22**, 325.
39 M. Lee and D. Kim, *BMC Bioinf.*, 2012, **13**, S6.
40 A. Lee, K. Lee and D. Kim, *Expert Opin. Drug Discovery*, 2016, **11**, 707–715.
41 T. Roy, S. T. Boateng, S. Banang-Mbeumi, P. K. Singh, P. Basnet, R.-C. N. Chamcheu, F. Ladu, I. Chauvin, V. S. Spiegelman, R. A. Hill, K. G. Kousoulas, B. M. Nagalo,

A. L. Walker, J. Fotie, S. Murru, M. Sechi and J. C. Chamcheu, *Bioorg. Chem.*, 2021, **107**, 104595.
42 Y. Lu, M. Tatsuka, H. Takebe and T. Yagi, *Mol. Carcinog.*, 2000, **29**, 1–7.
43 V. Vichai and K. Kirtikara, *Nat. Protoc.*, 2006, **1**, 1112–1116.
44 G. Huang, T. Cierpicki and J. Grembecka, *Bioorg. Chem.*, 2023, **135**, 106477.
45 A. K. Ghose, V. N. Viswanadhan and J. J. Wendoloski, *J. Comb. Chem.*, 1999, **1**, 55–68.
46 I. Muegge, S. L. Heald and D. Brittelli, *J. Med. Chem.*, 2001, **44**, 1841–1846.
47 D. F. Veber, S. R. Johnson, H.-Y. Cheng, B. R. Smith, K. W. Ward and K. D. Kopple, *J. Med. Chem.*, 2002, **45**, 2615–2623.
48 D. Lagorce, O. Sperandio, H. Galons, M. A. Miteva and B. O. Villoutreix, *BMC Bioinf.*, 2008, **9**, 396.